Extreme enrichment of selenium in the Apliki Cyprus-type VMS deposit, Troodos, Cyprus

Andrew J. Martin[1*], Iain McDonald[1], Christopher J. MacLeod[1], [Δ]Hazel M. Prichard[1] and Katie McFall[1]

[1]School of Earth and Ocean Sciences, Cardiff University, Main Building, Park Place, CF10 3AT, UK

[*]Corresponding Author: Martinaj4@cardiff.ac.uk

[Δ] Deceased

Abstract

The Troodos ophiolite Cyprus hosts the type locality for Cyprus-type, mafic volcanogenic massive sulphide (VMS) deposits. Regional soil geochemical data for Troodos are highly variable with the Solea graben, one of three regional graben structures on Cyprus, showing enrichment in Te and Se. Of the three VMS sampled within the Solea graben, Apliki exhibits the most significant enrichment in Se. Samples from the South Apliki Breccia Zone; a zone of hematite-rich breccia containing euhedral pyrite and chalcopyrite, contain up to 4953 and 3956 ppm Se in pyrite and chalcopyrite respectively. Four paragenetic stages are identified at Apliki and different generations of pyrite are distinguishable using trace element chemistry analysed via LA-ICP-MS. Results indicate stage I pyrite formed under reduced conditions at high temperatures >280 ˚C and contains 182 ppm (n=22 σ=253) Se. Late stage III pyrite which is euhedral and overprints chalcopyrite and hematite is enriched in Se (averaging 1862 ppm; n=23 σ=1394). Sulphide dissolution and hematite formation displaced large amounts of Se as hematite cannot accommodate high concentrations of Se in its crystal structure. The mechanisms proposed to explain the pronounced change in redox are twofold. Fault movement leading to localised seawater ingress coupled with a decreasing magmatic flux that generated locally

This is a 'preproof' accepted article for Mineralogical Magazine. This version may be subject to change during the production process.
DOI: 10.1180/mgm.2018.81.

oxidising conditions and promoted sulphide dissolution. Se/S ratios of 9280 indicate a probable magmatic component for late stage III pyrite which is suggested as a mechanism explaining the transition from oxidising back to reduced conditions. This study highlights the significance of changes in redox which promote sulphide dissolution, mobilisation and enrichment of Se.

KEYWORDS: mafic, VMS, selenium, Troodos Ophiolite, LA-ICP-MS, sulphides.

1. Introduction

Volcanogenic massive sulphide (VMS) deposits are important sources of base and trace metals, supplying 22% of the world's Zn, 6% Cu, 9.7% Pb, 2.2% Au, 8.7% Ag, and significant amounts of trace metals Co, Sn, Se, Mn, Cd, In, Bi, Te, Ga, and Ge (Franklin, 2005; Galley *et al.*, 2007). Despite their economic significance, the distribution and concentration of trace elements remains poorly constrained; this is especially true for critical elements tellurium (Te) and selenium (Se).

Tellurium and Se are extremely scarce in the crust (averaging just 1-4 ppb Te and 50 ppb Se) but are critical components used in photovoltaic solar cells (Grundler *et al.*, 2013; Perkins, 2011). Tellurium and Se are currently produced solely as by-products of Cu refining (Bustamante and Gaustad, 2014; Lu *et al.*, 2015). A predicted shift from pyrometallurgical to hydrometallurgical processing techniques accompanying a global decrease in Cu grades is expected to lead to a deficit in supply as hydrometallurgical techniques are not amenable to Te and Se extraction (Lu *et al.*, 2015; Moss *et al.*, 2013).

Because of the historical difficulties in analysing Te and Se at low concentrations, understanding of their distribution and mechanisms of enrichment in different geological environments remains poor. This includes primary mafic igneous systems and their associated metalliferous VMS deposits. In this paper we intend explore the distribution of the Te and Se within mafic ('Cyprus-type') VMS deposits in one of their principal localities, the Troodos ophiolite of Cyprus. This study begins to characterise

important processes in Se enrichment in Cyprus-type VMS systems and demonstrates that changes in redox and temperature may be significant in achieving enrichment to thousands of ppm levels.

1.1: Regional Geology

Cyprus is located in the eastern Mediterranean and consists of four main geological terranes: the Kyrenia Range, the Mesaoria plain, the Troodos Massif and (in SW Cyprus) the Mamonia Complex (e.g. Robertson and Xenophontos, 1993). The Troodos Massif is an ophiolite (Figure 1A) that represents a fragment of Turonian (~92 Ma ~~old~~) oceanic lithosphere formed during the closure of the Tethys ocean (e.g. Gass *et al.*, 1968; Robertson, 2002). Initially Troodos was considered to have formed in a typical (open-ocean) mid-ocean ridge (MOR) environment (Gass, 1980); however geochemical studies of the extrusive section demonstrate a geochemical affinity different from that of N-MORB, instead it is dominated by arc tholeiites and boninites (e.g. Robinson *et al.*, 1983; Rautenschlein *et al.*, 1985; Pearce and Robinson, 2010). Whereas it is now widely accepted that Troodos formed in a supra-subduction type setting, the exact nature of its geodynamic setting remains debated (Miyashiro, 1973; Pearce *et al.*, 1984; Pearce and Robinson, 2010).

Differential uplift occurred in the Neogene in response to serpentinisation (e.g. Robertson and Xenophontos, 1993) and led to the exposure of the complete ophiolitic crustal stratigraphy with relatively little deformation (Figure 1A). Zones of strongly epidotised dykes are believed to represent hydrothermal reaction zones (Richardson *et al.*, 1987; Jowitt *et al.*, 2012) and commonly occur in the lower sheeted dyke complex (SDC). At the periphery of the ophiolite and stratigraphically above the SDC is the extrusive sequence. The sequence consists of a 'Basal Group' transitional horizon that grades up into an aphyric 'Lower Pillow Lava' (LPL) suite characterised by evolved sheet flows and pillows of andesite/dacite composition. This is overlain by a more primitive suite of basaltic

andesitic, often olivine-phyric 'Upper Pillow Lavas' (UPL) (e.g. Gass *et al.*, 1994) (Figure 1A). This sub-division of the Troodos extrusive section is contentious and somewhat arbitrary. VMS deposits are found at different levels within the extrusive sequence and often occur at the contacts between the Basal Group/LPL or LPL/UPL (e.g. Adamides, 2010).

These issues notwithstanding, the relatively undeformed nature of the Troodos ophiolite, with preservation of original seafloor structures makes it an excellent location to investigate geochemical processes associated with VMS hydrothermal systems.

In-depth studies of the internal structure and spreading history of the Troodos ophiolite have revealed complexities in the mechanism of crustal accretion akin to processes recognised at modern slower-spreading mid-ocean ridges (e.g. Escartin and Canales, 2011). In particular, it is evident that tectonic stretching accompanied plate separation, such that normal faulting and tilting of upper crustal blocks (Figure 1B) occurred above a large-offset normal fault, the so-called Kakopetria Detachment (Varga and Moores, 1985; Nuriel *et al.*, 2009). This stretching of the SDC led to the formation of regional scale graben structures, defined by the 'bookshelf' faulting and tilting of SDC and lavas away from each other (Varga and Moores, 1985; Moores *et al.* 1990). From west to east these regional structures are defined as the Solea, Mitsero and Larnaca grabens respectively (Figure 1B).

The greater part of the extrusive section, comprising the UPL, LPL and upper Basal Group lithologies are extensively altered to zeolite facies (~150 ˚C) metamorphic assemblages with celadonite ($KMg_{0.8}Fe^{2+}_{0.2}Fe^{3+}_{0.9}Al_{0.1}Si_4O_{10}(OH)_2$) and natrolite ($Na_2Al_2Si_3O_{10}{\cdot}2H_2O$). The lower Basal Group marks a transition to greenschist facies metamorphic conditions (Gillis and Robinson, 1980). The vertical nature of dyke margins is an effective means for fluid to penetrate deep into the crust and as fluids descend to the base of the SDC they become heated to upper greenschist temperatures of ~350˚C; and at this point original mafic assemblages are replaced by epidote-quartz +/- titanite. Fluid inclusion (Bendnarz and Schmincke, 1990) and isotopic studies (Bickle and Teagle, 1992; Yamaoka *et*

al., 2015) support the pervasive and high temperature nature of hydrothermal alteration in the SDC. The transition from the sheeted dykes to upper plutonics marks a decrease in alteration intensity; fluid migrates laterally along the SDC-plutonic boundary before ascending through normal faults to the seafloor (Gillis and Roberts, 1999).

1.2: The Solea Graben

The Solea graben is a major tectonic lineament and represents a fossil spreading axis (Varga, 1991) (Figure 1B). Three significant VMS deposits are located in close proximity (~4 km) to the Solea axis: Skouriotissa (currently producing), Mavrovouni (exhausted) and Apliki (not currently producing).

The Solea graben is defined by a series of N-S trending normal faults controlling VMS distribution (Figure 1B). Skouriotissa is located closest to the inferred graben axis and is thought to be the youngest VMS deposit on the island; horizontal lava structure at Skouriotissa supports this observation as it has not undergone 'off axis' rotation. Apliki lies 4 km west of Skouriotissa within the LPL's and is inferred to have formed earlier than Skouriotissa as it is located further from the Solea axis and has experienced 'off axis' rotation (see section 4.2).

2. Cyprus-type VMS

2.1 VMS Formation and Morphology

Troodos hosts the type locality for Cyprus-type VMS deposits (Cox and Singer, 1986). Cyprus-type VMS may also be classified as either mafic (Galley *et al.*, 2007) or Cu-(Zn) (Franklin *et al.*, 2005). But for the purpose of this paper we retain the original name.

Cyprus-type VMS are hydrothermal ore deposits derived from the interaction of evolved seawater with mafic country rocks under greenschist facies metamorphic conditions (350 ˚C). Cold (2 ˚C), oxidised seawater reacts with volcanic glass which lowers pH as it enters the sub-surface through cracks and fissures (Seyfried Jr. and Mottl, 1982) (Figure 2). The fluid continues to migrate

downwards into the SDC and becomes superheated to 350-400 ˚C with a pH of around 2; at this point exchange occurs between the fluid and host rock forming epidosites (Gillis and Robinson, 1980; Jowitt *et al.*, 2012) (Figure 2). Epidosites are widely accepted as a source of base and trace metals in Cyprus-type VMS of Troodos (Jowitt *et al.*, 2012; Schiffman *et al.*, 1990; Seyfried and Bischoff, 1977).

Metal laden hydrothermal fluid rises through normal faults that provide a permeability pathway and focal mechanism channelling fluids to the seafloor (Figure 2). Upon exhalation, hot reduced fluid mixes with seawater leading to ligand disassociation (Cl^-, HS_2^-), the precipitation of sulphides and VMS formation (Humphris and Cann, 2000).

Cyprus-type VMS are relatively low tonnage averaging 2.8 Mt (n=62) but high grade with >2 wt.% Cu (Barrie, 1999; Hannington *et al.*, 1998). They are Zn and Pb poor with average grades of <0.7 wt.% and <0.1 wt.% respectively (e.g. Adamides, 2010); reflecting the mafic host rock, lack of sediments and absence of felsic volcanics leading to a depletion in Pb relative to Cu (Tornos *et al.*, 2015). Tonnages of VMS in Troodos range from <0.05 Mt to >16 Mt (Adamides, 2011, 2010).

Exhalative ore bodies are characterised by a strataform lens of cupriferous pyrite with a typical mound morphology (e.g. Phoucasa or Mala). Massive pyrite exhibits vuggy, colloform or sandy textures grading to semi-conformable Cu-rich stockwork at depth. For some deposits no clear evidence for exhalation is visible as they lack colloform/banded textures, chimney fragments or vent fauna suggesting they may have formed via subseafloor replacement (Doyle and Allen, 2003). Mineralogy is dominated by pyrite (euhedral to colloform), chalcopyrite and sphalerite with inclusions of galena and abundant Cu secondaries, covellite, digenite and chalcocite (Adamides, 2010, 2011). Alteration surrounding the VMS is characteristically silica and chlorite dominated with disseminated pyrite.

2.2 Te and Se Systematics in VMS

Pyrite is ubiquitous with many hydrothermal ore deposits and may contain substantial concentrations of trace elements (e.g. Huston *et al.*, 1995; Revan *et al.*, 2014). Trace elements in VMS commonly occur in three forms: (i) discrete mineral phases (e.g. tellurides or selenides), (ii) in a solid solution within the crystal lattice or (iii) micro-nano inclusions (Huston *et al.*, 1995; Layton-Matthews *et al.*, 2008; Revan *et al.*, 2014).

Trace elements may be classified into three categories based on their behaviour during incorporation into pyrite (Huston *et al.*, 1995). Group (i) occur as inclusions (Cu, Zn, Pb, Ba, Bi, Ag and Sb), group (ii) in non-stoichiometric substitution (As, Tl, Au and Mo) and group (iii) as a stoichiometric substitution for S (Se and Te) or Fe (Co and Ni) (Huston *et al.*, 1995). Huston *et al.*, (1995) state that both Te and Se are incorporated via stoichiometric substitution with S ions; this however seems unlikely for Te given its larger ionic radius (2.42 Å) compared with S (2.14 Å) (e.g. Butler and Nesbitt, 1999; Rahm *et al.*, 2016). In contrast Se has a similar ionic radius to S at 2.24 Å (Butler and Nesbitt, 1999; Maslennikov *et al.*, 2009; Rahm *et al.*, 2016).

The process of substitution is influenced by the physiochemical properties of the hydrothermal fluid, resulting in the highly variable distribution of Te and Se in pyrite (Butler and Nesbitt, 1999; Genna and Gaboury, 2015; Huston *et al.*, 1995). Increased Te concentrations in the inner wall of vent chimneys from the Broken Spur vent field at 29° on the Mid Atlantic Ridge suggest Te is more readily incorporated at high temperatures (Butler and Nesbitt, 1999). High temperatures also favour the incorporation of Se as the Gibbs free energy of mixing becomes increasingly more negative at higher temperatures allowing the lattice structure to tolerate higher concentrations of Se (Maslennikov *et al.*, 2009). Theoretically this should lead to enrichment of Se and Te in high temperature zones of a VMS (e.g. stockwork) (Maslennikov *et al.*, 2009).

Modelling by Huston *et al.* (1995) argues that Se incorporation is enhanced at low temperatures (Figure 3). At temperatures <200 ˚C Se incorporation in pyrite is controlled by redox and pH whereas at temperatures >200 ˚C Se incorporation is controlled by fluid H_2Se/H_2S ratio and temperature

(Huston *et al.*, 1995). In hydrothermal fluids above 200 ˚C H_2Se/H_2S are the dominant species and thus approximate to Se/S ratios (Huston *et al.*, 1995). At temperatures >300 ˚C the ratio of H_2Se/H_2S in the hydrothermal fluid is constant, equating to uniform Se concentrations in pyrite of 200-250 ppm and Se/S ratios of 10^{-4} (Figure 3) . By contrast, at 150 ˚C the concentration of Se in equilibrium with the hydrothermal fluid is more variable leading to Se enrichment in pyrite up to a theoretical value of 100,000 ppm (Huston *et al.*, 1995).

3. Sampling and Methods

To investigate the spatial distribution of Te and Se within southern Cyprus and the Troodos ophiolite in particular, we first obtained regional soil geochemical data from the Geological Survey Department of Cyprus (GSD) (see Cohen *et al.*, 2012). Sampling was carried out by the GSD using a nominal grid size of one sample per 2.2 km² for Troodos and 1 km² for surrounding sedimentary units (Cohen *et al.*, 2012). Two sampling depths were investigated: top soil (Figure 4), sampled at a depth of 0-25 cm, and subsoil sampled at 50-75 cm depth. An aqua regia digest followed by ICP-MS analysis for trace elements and XRF for major elements was used (Cohen *et al.*, 2012). Detection limits were 0.01 and 0.1 ppm for Te and Se (via ICP-MS).

Follow up samples for this study were collected during field seasons in 2016 and 2017. All samples obtained from Apliki were *in-situ* (i.e. not from spoil heaps) from the surface sampling of pit faces. Apliki has been historically mined leading to the exposure of different ore horizons within the open pit providing a cross-section through the lower regions of VMS mineralisation. Sample locations from this study are summarised in Table 1.

Portable X-ray Fluorescence (P-XRF) analysis was carried out on 640 powdered samples from VMS and mineralised areas across Troodos, 26 of which were from Apliki. Samples were crushed using a jaw crusher and powdered using a tungsten carbide TEMA mill. Twenty grams of sample were then

pressed into a plastic vessel with a Mylar cover slip (3µm thickness) ready for analysis. Analysis was performed using an Olympus Delta Professional P-XRF analysed in Geochem mode for 60 seconds to determine Mg, Al, Si, P, S, K, Ca, Ti, V, Cr, Mn, Fe, Co, Ni, Cu, Zn, As, Se, Rb, Sr, Y, Zr, Mo, Ag, Cd, Sn, Sb, W, Hg, Pb, Bi, Th and V. Te was not analysable. Data quality was monitored by the repeat analysis of standards KPC1, SU1A and a silica blank every twenty samples.

Following the initial screening of 26 samples from Apliki via P-XRF, seven representative samples containing elevated whole rock Se (>50 ppm) were selected for mineralogical and textural characterisation using reflected light microscopy followed by X-ray diffraction analysis.

X-Ray Diffraction analysis was carried out on powdered sample APL-1 to confirm dominant Fe matrix phase(s). A scan was run using the Philips PW1710 Automated Powder Diffractometer using Cu Ka radiation at 35kV and 40mA, between 2 and 70 ˚2θ at a scan speed of 0.04 ˚2θ /s. Each sample was identified using Philips PC-identify software.

Variations in trace elements within sulphides were determined by Laser Ablation Inductively Coupled Plasma Mass Spectrometry (LA-ICP-MS). 150 spot analyses were performed on pyrite and chalcopyrite from seven polished blocks. The isotopes analysed include ^{57}Fe, ^{65}Cu, ^{59}Co, ^{66}Zn, ^{75}As, ^{77}Se, ^{109}Ag, ^{111}Cd, ^{121}Sb, ^{125}Te, ^{185}Re, ^{189}Os, ^{193}Ir, ^{195}Pt, ^{197}Au ^{206}Pb and ^{209}Bi (see Appendix). ^{77}Se was used for Se analyses due to lower levels of interference from the ablation gas compared to ^{82}Se. Analysis was performed using a New Wave Research UP213 UV laser system coupled to a Thermo X Series ICP-MS (Cardiff University). Samples were analysed in time-resolved mode using a spot diameter of 55 µm and 80 µm (depending on sulphide grain size) with a frequency of 10 Hz. Acquisition lasted 45 seconds and a gas blank was measured for 20 seconds prior to the start of analysis. ^{33}S was used as an internal standard for all analyses and subtraction of gas blanks and internal standard corrections were performed using Thermo Plasmalab software (Prichard *et al.*, 2013).

Detection limit for Se varied from 9-15 ppm for the different analytical runs due to mass interference associated with the Ar/Cl gas during ablation. This variation in detection limit does not affect the data significantly as a large proportion of Apliki samples contained >50 ppm Se.

4. Results

4.1: P-XRF Anomaly Identification

Regional soil geochemistry (GSD data set) highlights the variable distribution of Te and Se in the soils of Cyprus (Figure 4). P-XRF data for Se shows that VMS deposits of the Solea graben are enriched relative to other VMS of Troodos (Figure 4). Data displayed in Figure 4 are for topsoil transects only (0-25 cm). The interpolated surface uses point data. Classification into 12 categories is arbitrary as geochemical data has been rounded to one decimal place making it difficult to detect natural and more meaningful variation. Nevertheless, the data are useful in highlighting areas of enrichment which may otherwise be overlooked. Figure 4 (Se transect A) benefits from the addition of P-XRF data for Se. The distribution of Te and Se from soil data is highly variable throughout Troodos with Te and Se data highlighting mine sites, especially the Limni, Kalavasos, Skouriotissa and Mala VMS (red circles- Figure 4). All four mines have significant spoil heaps associated with mining activities. Disturbance of sulphide waste leads to the mobilisation of Te and Se into the surrounding soils and the dispersion of Se into the environment creating wider anomalies.

Regional geochemical data and P-XRF anomalies highlight elevated Te and Se within the Solea graben. Two of three deposits in the Solea graben; Mala and Skouriotissa show elevated Te and Se from regional soil chemistry data (Figure 4). Apliki is not highlighted by regional soil data, most likely due do its location within the UN buffer zone making it difficult to access, the nearest soil survey point is 0.5 km south of Apliki. Sulphide samples analysed in this study are some of the first since the 1974 ‘Green Line’.

Out of 640 samples screened via P-XRF from VMS and mineralised localities across Troodos, samples at Apliki were relatively enriched with Se ranging from below detection <12 ppm to 1071 ppm (n=26). By comparison the highest value recorded for Skouriotissa was just 141 ppm Se. P-XRF identified samples from the South Apliki Breccia Zone as containing the highest concentrations of Se (between 970-1071 ppm) representing a significant whole rock enrichment when compared to other VMS in Troodos.

4.2: The Apliki VMS

Apliki is owned by Hellenic Copper Mines and although the deposit is not currently mined potential exists for future extraction of stockwork ore. We interpreted Apliki based on historic data and new field observations to be a 'typical' Cyprus-type VMS; a cupriferous stockwork overlain by a massive sulphide lens. The exhalative interpretation relies heavily on historic data as no massive sulphide remains. Adamides (2010) report an average Cu grade of 1.6 wt.% and total tonnage of 1.6 Mt (mainly exhalative ore). The mineralised VMS package is bound by normal, axis parallel (N-S- 350˚) faults dipping 50-55˚ to the east (towards Solea axis- Figure 5A and 5B); the hanging wall contains westward dipping (36-52˚) 1-3 m thick flow units (Figure 5A and 6). The contact on both parallel bounding faults is sharp; mineralisation does not cross the contact suggesting a degree of post mineralisation fault movement. The footwall unit is highly degraded and the extent of rotation less clear but flows have been measured dipping 34˚ west. The footwall morphology is dominated by pillows and hyaloclastites not flows and celadonite abundance increases dramatically indicating a higher temperature of formation and that the footwall formed stratigraphically deeper than the hanging wall (i.e. the fault therefore has a normal geometry). The mineralised fault bound zone is approximately 100 m wide and consists of silicified, chloritised brecciated LPL with disseminated pyrite (2-5 modal %) and no massive sulphide mineralisation (Figure 5A and 6). The lower northern wall region is chalcanthite and azurite rich.

At the southern end of the pit, fresh sulphide is preserved and material is best accessed via a drainage gully in the centre of the lowermost bench (Figure 5B). The area is rich in coarse grained semi-massive pyrite with an unusual hematite-(magnetite)-chalcopyrite-pyrite rich breccia zone (Figure 7). In this zone chalcopyrite is more abundant than pyrite accounting for up to 70 wt.% of samples collected (Figure 6 and 7). From this point the zone will be termed the South Apliki Breccia Zone. The breccia zone is continuous for 4-5 m (depth) in cross-section through two bench levels and only well exposed perpendicular to strike for 2-3 m. Within this relatively narrow zone several morphological distinctions can be made based on modal mineralogy and degree of silicification (Figure 7 and Table 1). Hematite also occurs in discrete cm wide veins which crosscut pillows in the footwall. Chalcanthite, covellite and azurite are abundant in the southern pit wall (Figure 7).

The hematite breccia is somewhat unique to the Apliki VMS and although specular hematite is common within pseudo-epithermal 'T' type mineralisation in Troodos defined by Jowitt *et al.* (2005) (e.g. at Alestos or Touronja) to our knowledge it does not coexist with large amounts of chalcopyrite at any other locality.

4.3: Mineralogy of South Apliki Breccia Zone

Reflected light microscopy on seven representative polished blocks from the South Apliki Breccia Zone (Figure 8) reveals four stages of paragenesis (summarised in Table 1 and Figures 8, 9 and 10). Generally, chalcopyrite is variably altered to covellite and digenite at grain boundaries. Pyrite, when present is idiomorphic and may be replaced by hematite (Figure 8 and 9). Semi quantitative XRD (Appendix) indicates that hematite is the dominant matrix phase occurring in both specular form and mixed with silica as jasper (optically identified). Subsequently samples are grouped into four alteration stages based on pyrite morphology and degree of hematite and covellite alteration.

Stage I samples (APL-5 and APL-7) contain significant amounts of chalcopyrite that exhibits no visible oxidisation along grain boundaries. Critically pyrite is subhedral to anhedral and does not overprint chalcopyrite. Pyrite is readily preserved rimming chalcopyrite and is rarely altered to hematite

(Figure 8 and 9). This stage of alteration is characterised by a hematite matrix (55%) with 1-2 mm subhedral pyrite (20 %) and chalcopyrite (20 %). Pyrite is heavily pitted and commonly observed rimming chalcopyrite. Very few pyrite grains are euhedral; euhedral grains occur overgrowing chalcopyrite whilst subhedral pyrite appears cogenetic and do not overgrow chalcopyrite. Dissolution features are rare occurring only in a small number of pyrite grains (<5 %) where pyrite is locally altered to hematite (Figure 8 and 10).

Stage II samples (APL-2 and APL-3) contain large amounts of hematite forming botryoidal to acicular masses within the matrix. Pyrite is less common than in stage I forming both subhedral grains (<2 mm) and euhedral grains >2 mm. Chalcopyrite is minor compared to stage I and may be altered to covellite and digenite (Figure 10 and 11).

The third stage of ore formation is well developed in samples APL-1 and APL-6; euhedral coarse pyrite overprints both chalcopyrite and the hematite-goethite matrix. Euhedral pyrite which overprints earlier phases exhibits no hematite alteration suggesting they formed during in the last stage of mineralisation. Stage III alteration comprises roughly equal proportions of hematite (40 %) and chalcopyrite (40 %) with minor pyrite (20 %) which is coarse grained (1-3 mm) and euhedral. Chalcopyrite is interstitial surrounding pyrite and in some areas forms crystals up to 6 mm (Figure 8). Chalcopyrite may be oxidised to covellite and digenite (Figures 9, 10 and 11).

Supergene alteration of chalcopyrite produces dominantly covellite + diginte +/- chalcocite with goethite. Alteration is generally limited to grain boundaries and rarely in stage IV samples grains may be completely dissolved or replaced (Figure 8 and 9). Stage IV alteration is characterised by a fine matrix of botryoidal to acicular hematite with variable amounts of jasper. Pyrite is a minor constituent (20 %) limited to bands of specular hematite. Pyrite exhibits a subhedral to rounded morphology and may be coarse up to 3 mm. Chalcopyrite is a minor constituent (<10 %) forming globular masses 1-5 mm and is rarely overgrown by pyrite. Covellite if present rims chalcopyrite and upon weathering is preserved as a series of sub-rounded voids which indicate relict chalcopyrite-

covellite grains. Reaction rims forming Cu secondaries around the margin of chalcopyrite are generally 20-30 µm (Figure 8 and 9).

Magnetite is not readily preserved in any samples at Apliki with hematite forming the major oxide phase (XRD- Appendix). Very few grains of pyrite show evidence of hematite replacing pyrite but rarely radial growths of hematite can replace pyrite cores (Figure 8). Within the hematite-goethite matrix cubic pyrite pseudomorphs are common (Figure 9).

4.4: LA-ICP-MS of Sulphides

A total of 150 LA-ICP-MS spot analyses from Apliki, 96 of pyrite and 54 of chalcopyrite were analysed in seven representative polished blocks. Te and Se maximum values in pyrite reach 70 and 4943 ppm respectively. LA-ICP-MS of sulphides from Apliki indicate that Te and Se concentration varies systematically with alteration stage. Se within pyrite varies enormously from <15 (below detection limit) to 4953 ppm. Similar variation is observed in chalcopyrite with Se concentrations ranging from 104 to 3956 ppm. The average Se concentration in chalcopyrite is typically 700 ppm, greater than pyrite at 1576 ppm (n=54) (summarised in Table 2- See Appendix A).

Bivariate plots of Te and Se against other trace elements from LA-ICP-MS data are shown in Figure 12 (see Appendix). Te and Se exhibit no clear correlation (R^2=0.02) suggesting a decoupled behaviour during VMS formation. Se exhibits limited correlation with all trace elements, whereas Te exhibits a weak positive correlation with Bi (R^2=0.3) and Co (R^2=0.2) but no corelation with As (R^2=0.01).

Arsenic is low in the South Apliki Breccia Zone averaging just 152 ppm in pyrite compared with 496 ppm for all other deposits in Troodos (Table 3) . Co concentration in pyrite is similar to the mean value for all deposits at 245 ppm and 268 ppm for Apliki (Table 3). Bi concentration in pyrite is lower in Apliki at 2.46 ppm compared with all other VMS but marginally higher when compared to Skouriotissa at 1.66 ppm (Table 3). A comparison of average trace element concentrations for Apliki and all other VMS of Troodos is summarised in Table 3 (all data in Appendix).

When comparing between chalcopyrite and pyrite clear trends exist (Table 2 and 3). Chalcopyrite is enriched in Se relative to pyrite but depleted in Te, As, Co and Bi. Similar trends exist when comparing the relative concentration of elements between pyrite and chalcopyrite for all VMS considered in this study (Table 3). Co is elevated at Skouriotissa for both pyrite and chalcopyrite at 406 ppm and 72 ppm respectively compared to 268 and 4.96 ppm for Apliki (Table 3). Se in chalcopyrite in all VMS excluding Apliki and Skouriotissa is significantly lower than that recorded at Apliki (Table 3).

5. Discussion

5.1: Range of Se Concentrations in VMS

The South Apliki Breccia Zone appears unique within Troodos in both its mineralogy and unusual enrichment in Se. Very little trace element data (particularly Te and Se) exists for Cyprus-type VMS and especially VMS within Troodos. One study by Keith *et al.* (2016) on the Skouriotissa VMS, located near Apliki within the Solea Graben (see Figure 5A) shows that Se concentration apparently exhibits systematic variation with depth in the ore body; deeper levels being more enriched (Keith *et al.*, 2016). Maximum Se and Te values in pyrite in Skouriotissa analysed via LA-ICP-MS are 1886 and 53 ppm respectively and correspond to euhedral pyrite from deep-stockwork (Keith *et al.*, 2016). The average Se content from euhedral pyrite in Skouriotissa's most enriched deep-stockwork zone is 948 ppm (Keith *et al.*, 2016). Te is comparable to values measured in Apliki ranging from 0.7-12 ppm compared to 4-16 ppm with a maximum of 70 ppm at Apliki. By comparison Se exhibits a much greater enrichment in the South Apliki Breccia Zone averaging 182 (n=22) and 1862 (n=23) ppm in

stage I and III pyrite respectively. Maximum values for Se are significantly higher at Apliki reaching 4953 ppm in pyrite. Other Cyprus-type deposits exhibit a wide variation in Se content from 20 ppm in the Mathiati North VMS of eastern Troodos (Economou-Eliopoulos *et al.*, 2008) to 177 and 1 ppm Se in the chalcopyrite and sphalerite rich zones of the TAG deposit (Mid Atlantic Ridge) (Hannington *et al.*, 1998).

Greater volumes of data exist for VMS deposits formed in bi-modal environments. Three notable Canadian examples which exhibit unusual enrichment in Se are outlined; the Finlayson Lake District (Layton-Matthews *et al.*, 2013), Bracemac-McLeod (Genna and Gaboury, 2015) and Kidd Creek (Hannington *et al.*, 1999).

Selenium enrichment analysed via LA-ICP-MS of sulphides from the Bracemac-McLeod deposit occurs in type IV late recrystallized pyrite with a maximum Se content of 1059 ppm. The maximum Se concentration of 4900 ppm in chalcopyrite is comparable to the 3955 ppm recorded at Apliki (Genna and Gaboury, 2015). Layton-Matthews *et al.* (2013) note Se enrichment in 'type-1' pyrite samples from the chalcopyrite rich zone (Wolverine deposit) with values of up to 3400 ppm. Average Se values for the Wolverine deposit are 1100 ppm. Se is also reported to be enriched in the bornite zone of the Kidd Creek deposit (Hannington *et al.*, 1999). Se whole rock concentrations from the 'Se rich halo' average 500 ppm whilst the bornite zone exhibits average concentrations of 2200 ppm. Hannington *et al.* (1999) also report Se enrichment up to 0.8 wt.% in pyrite. However, higher average whole rock Se on a deposit scale in bi-modal VMS is attributed to the presence of galena-clausthalite (Pb-S-Se); this does not explain the higher *in situ* Se content of pyrite at the Apliki VMS.

As and Se concentrations at Apliki are more comparable to those recorded in bi-modal VMS than for other Cyprus-type deposits; a mechanism of Se enrichment is needed to explain such enrichment compared with other Cyprus-type deposits. Bi-modal deposits are preferentially enriched as a function of their felsic source rock, an additional magmatic component or high galena-clausthalite contents.

The South Apliki Breccia zone is significantly enriched in Se with maximum values of 3956 ppm Se in chalcopyrite and 4953 ppm Se in pyrite. These values are substantially higher than any other values reported for Cyprus-type VMS. Concentrations are an order of magnitude higher than those reported for chalcopyrite in the TAG mound (177 ppm; Hannington *et al.*, 1998) and four times higher than maximum values reported by Keith *et al.* (2016) for the Skouriotissa ore body.

5.2: The Source of Se in VMS Deposits

A magmatic influx into the VMS hydrothermal system via vapour or aqueous phase transfer has long been hypothesised to explain enrichment in certain magmatophile elements e.g. Se, Te, Cu, Bi, Co etc. (Chen *et al.*, 2015; Melekestseva *et al.*, 2017; Sillitoe *et al.*, 1996). The $\delta^{34}S$ values for most MOR and back-arc VMS sulphides falls within a narrow range of 0 to 5 ‰ $\delta^{34}S$. The narrow range reflects the mixing of magmatic sourced sulphur (0 ‰- Vibetti, 1993) and sulphur derived from seawater sulphate reduction (+20.7 ‰, Herzig *et al.*, 1998; Vibetti, 1993). Increased magmatic influx leads to a decrease in $\delta^{34}S$ values toward 0 ‰. A modern analogue of an 'end member' magmatic VMS may be found in the Lau Basin, Tonga-Kermadec Arc at the Hine Hina vent site (Herzig *et al.*, 1998). Sulphides from Hine Hina exhibit the lowest $\delta^{34}S$ of any modern hydrothermal field at -5.3 ‰ (Herzig *et al.*, 1998). The variable $\delta^{34}S$ of modern seafloor sulphide deposits demonstrates that the source of metals in VMS systems is varied, and when considering elements of magmatic affinity (Se, Te, Cu, Bi, Co) volatile transfer from the magmatic to hydrothermal system may be important in their enrichment.

Although outside the scope of the current study, limited $\delta^{34}S$ data does exist for the Skouriotissa VMS and suggests a variable magmatic influx in the Solea graben (Keith *et al.*, 2016). Deep stockwork ore exhibits a light $\delta^{34}S$ signature of -1.4 ‰, a figure unobtainable through the mixing of Cretaceous seawater (+18-19 ‰) and primary magmatic derived S (0 to -1 ‰) (Keith *et al.*, 2016). The shallow stockwork at Skouriotissa exhibits a positive $\delta^{34}S$ signature of +6.1 ‰ suggesting an increased

seawater source of S in the upper VMS stratigraphy (Keith *et al.*, 2016). The negative $\delta^{34}S$ value in deep stockwork may represent a magmatic volatile input.

S/Se ratios are used as a proxy for the source of sulphide mineralisation in a range of environments (e.g Graham *et al.* 2017; Layton-Matthews *et al.* 2013; Holwell *et al.*, 2015). More commonly when considering VMS systems Se/S ratios are used (expressed as Se/S x 10^6) (Layton-Matthews *et al.*, 2008). Chemical similarities between S and Se and the contrasting ratio of Se:S in seawater, mantle sulphides and sediments are used to infer the source of Se in ore deposits (Huston *et al.*, 1995; Layton-Matthews *et al.*, 2008, Hannigton *et al.*, 1999). Sulphides with high Se/S (>500) ratios are inferred to have a magmatic source (primitive mantle ~300), whereas low Se/S (<500) ratios indicate a sedimentary or seawater origin (Huston and Large, 1989; Layton-Matthews *et al.*, 2008; Hannington *et al.*, 1999). S/Se of pyrite from the South Apliki Breccia Zone are summarised in Figure 13.

Se/S ratios from the South Apliki Breccia Zone used as a proxy for magmatic influx exhibit systematic variation with alteration stage. Stage I samples fall below the proposed seawater-magmatic discrimination line (Se/S 500 Layton-Matthews *et al.*, 2008) whilst stage II are highly variable and stage III samples plot in the magmatic region (>>500). Stage IV samples exhibit significant scatter plotting in both the seawater and magmatic domains; this may be a function of supergene processes which lead to the mobilisation of S during oxidisation relative to Se or vice versa. The data suggests a change in source from seawater to magmatic with alteration intensity (discussed in section 5.4). Further $\delta^{34}S$ analysis which is outside the scope of the present study is needed to confirm the suggested presence of any late magmatic influx at the Apliki VMS.

Se/S ratios vary significantly with alteration stage in the South Apliki Breccia Zone; Se/S values range from 24 in stage I pyrite to 9238 in stage III pyrite (Figure 13). Layton-Matthews *et al.* (2008) state that Se/S ratios for sediment starved ridges such as Troodos are <1500. Forty four of 96 analyses are above the 1500 threshold suggested by Layton-Matthews *et al.* (2008). Two different mechanisms

have been proposed to explain elevated Se/S ratios; a sediment source similar to the Wolverine deposit e.g. sulphide rich shales (Se/S- 38700 Layton-Matthews *et al.*, 2008) or a magmatic volatile input (e.g. Kidd Creek, Hannington *et al.*, 1999).

No sediment relating to ophiolite formation has been documented in the Troodos stratigraphy (e.g. Robinson and Malpas, 1987), therefore it is unreasonable to assume that Se/S ratios have been significantly modified by sediment-hydrothermal fluid interaction. The transition in Se/S ratios between stage I and III samples suggests a late magmatic influx into the hydrothermal system at Apliki providing one plausible mechanism explaining the enrichment of Se in late stage III pyrite. Hannington *et al.* (1999) report high Se/S values (20,000-50,000) for the bornite-rich zone at Kidd Creek that they attributed to a magmatic influx of H_2Se leading to significantly higher Se/S ratios.

It should be noted that as with previous studies (e.g. Graham *et al.* 2017) a stoichiometric value for S within pyrite of 53.5 % has been used to calculate Se/S ratios. Actual S concentrations will vary by a few % around this value, however, the observed trends are expected to prevail.

In addition to a probable magmatic source of metals in the VMS hydrothermal system, base and trace metals are mobilised from epidosite zones (Jowitt *et al.*, 2012; Patten *et al.*, 2017; Schiffman *et al.*, 1990). Mass balance calculations suggest the epidosite zones of the Solea graben are capable of mobilising enough metal to form a medium sized VMS deposit (Jowitt *et al.*, 2012; Patten *et al.*, 2017).

Studies by Jowitt *et al.* (2012) demonstrate the significance of epidosite zone formation in fulfilling metal budgets for VMS in supra-subduction settings. Similarly, the findings of Patten *et al.* (2017) demonstrate the importance of epidosite zones in the Se budget with a 90 % depletion in Se when compared to cogenetic volcanic glass (Patten *et al.*, 2017). Using an average Se concentration of 41 ppm for Cyprus-type VMS and a theoretical hydrothermal reaction zone of 10.9 km^2 (5 km^2 epidosite and 5.9 km^2 diabase), it is estimated that 3100 ± 700 t Se was mobilised in the Solea graben (Patten *et al.*, 2017). If this was the case higher average Se would be expected in VMS of Troodos. Trapping

efficiencies are suggested to account for the low Se content of Cyprus-type VMS with only 27 % of all mobilised Se being trapped in VMS (Patten *et al.*, 2017).

The bulk Se content of VMS in Troodos is poorly constrained with Patten *et al.*, (2017) reporting average compiled data values of 41 ppm, whilst in this study we find an average of 55 ppm in pyrite (n=345) and 77 ppm (n=20) in chalcopyrite excluding the extreme values recorded at Apliki. It is unclear from Patten *et al.*'s (2017) study if the mineral scale distribution of Se is considered in mass balance calculations. As demonstrated in this study the mineral scale distribution of Se favours chalcopyrite with average Se contents of 77 and 315 ppm for all Troodos deposits and Skouriotissa respectively. Taking the mineral scale distribution of Se into account, the trapping efficiency of Se is likely to be higher than the 27 % reported by Patten *et al.* (2017).

While it is likely that Se is mobilised largely from epidosite zones as suggested by Patten *et al.* (2017), VMS which are unusually rich in Se such as Apliki and Skouriotissa may have an additional source of enrichment, possibly through a magmatic volatile influx.

5.3 Mineral Scale Distribution of Te and Se

Data from this study highlights the correlation between Te and so called 'lattice modifying elements'. Lattice modifying elements increase the substitution potential of large ions such as Te and of particular interest, ions exhibiting moderate positive correlation with Te (refer to section 4.4) are Bi and to a lesser extent Co (Figure 12). Arsenic concentrations are low within Apliki averaging 152 ppm (pyrite, n=96) compared with all other Cyprus VMS sulphides (Table 3) which average 469 ppm (n=195). No correlation exists between As and Te suggesting it is not important in the substitution of Te in the Apliki VMS.

Selenium is preferentially incorporated into chalcopyrite over pyrite with an average concentration of 922 (n= 96) and 1576 (n=54) ppm in pyrite and chalcopyrite respectively. Se contents of chalcopyrite from the South Apliki Breccia Zone average 601-2215 ppm whilst Te is just 4-8 ppm

(n=54). By comparison Te is elevated in pyrite relative to chalcopyrite at 8-16 ppm (n=96). These observations agree with thermodynamic data that indicate increased affinity for Se decreasing in concentration from galena-claushalite >> chalcopyrite > sphalerite > pyrite > pyrrhotite (Layton-Matthews *et al.*, 2008). Despite high Se concentrations within sulphides at Apliki no selenide phases have been identified suggesting Se is incorporated solely in sulphide minerals. Incorporation of Se is likely accomplished through stoichiometric substitution of Se for S (Maslennikov *et al.*, 2009).

5.4 Physiochemical Factors Effecting the Incorporation of Te and Se

The Apliki mineralogy is dominated by chalcopyrite indicating mineralisation temperatures of 280-350 ˚C (e.g. Gill *et al.*, 2016; Safina *et al.*, 2016) (Figure 14, stage I). The increased incorporation potential of Se at high temperatures is not supported by low average Se in chalcopyrite (601 ppm, n=12) and pyrite (182 ppm, n=22) from early stage I sulphides at the South Apliki Breccia Zone. In contrast, stage III pyrite contain an average of 1862 ppm (n=23) Se and formed at lower temperatures (<280 ˚C). Temperature alone does not explain the significant enrichment of Se in stage III sulphides over stage I sulphides at Apliki. Samples analysed from the South Apliki Breccia Zone represent the highest Se values not only at Apliki, but the whole of Troodos and to our knowledge Cyprus-type VMS in general. They occur in a distinct zone not recorded in any other Cyprus-type VMS system on Troodos. The zone exhibits textural and mineralogical similarities to the Alestos deposit of north-central Troodos; a deposit thought to have formed from late, low temperature oxidised fluids (Eddy *et al.*, 1998; Jowitt *et al.*, 2005). Brecciation, silicification and chloritisation with abundant hematite are common features between the two deposits however Se analyses from Alestos were below detection limit (LA-ICP-MS pyrite, n=5). The similarity in mineralogy suggests a late, low-temperature, oxidising fluid may be responsible for hematite formation in the South Apliki Breccia Zone however a more complex paragenesis is needed to explain the enrichment in Se.

The Ortaklar VMS Turkey is a comparable analogue to the South Apliki Breccia Zone as it has a late oxidised overprint (Yildirim *et al.*, 2016). No Te or Se data were presented in the latter study however similarities in ore texture and mineralogy suggest the two deposits share a similar paragenesis. At Ortaklar magnetite crosscuts high temperature hypogene chalcopyrite ore. Yildirim *et al.* (2016) envisage two stages of ore formation; an early high temperature pyrite and chalcopyrite dominated phase involving, reduced, hot, low pH fluids (e.g. Tornos, 2006) and a second stage of magnetite formation. Increasing fO_2 promoted the dissolution and replacement of sulphides with magnetite, hematite and specularite and the oxidisation of chalcopyrite (Yildirim *et al.*, 2016).

The South Apliki Breccia Zone and Ortaklar exhibit paragenetic sequences indicative of multiple mineralising phases under varied but different redox conditions (Figure 14). At Ortaklar magnetite is the main secondary mineral whereas at Apliki hematite is dominant. Fluids at Apliki are inferred to be of lower pH with a log fO_2 less than -30 to -40 at >300 ˚C promoting the precipitation of hematite over magnetite (Figure 14: stage II/III) (Galley *et al.*, 2007). Hematite could also have formed during supergene oxidation of magnetite ($4\ Fe_3O_4 + O_2 = 6\ Fe_2O_3$) however a purely supergene origin for hematite is not likely as fresh euhedral pyrite is preserved in an entirely hematised matrix. This suggests ore formation remained active after the formation of hematite. If hematite were solely a supergene phase, pyrite and chalcopyrite would be extensively oxidised, dissolved or completely absent, and this is not observed.

A similar paragenesis of replacement over precipitation of new mineral phases is proposed for the Ortaklar VMS (Yildirim *et al.*, 2016). Exsolution and zoned textures are common at Ortaklar indicating replacement of early stage mineralisation under varied temperature and redox conditions (Yildirim *et al.*, 2016). At Ortaklar magnetite represents the last stage in VMS mineralisation (Yildirim *et al.*, 2016) whilst at Apliki both hematite and chalcopyrite are overprinted by euhedral pyrite. The formation of stage III pyrite suggests a temporary influx of oxidised fluids that reverted back toward more reducing conditions and sulphide precipitation (Figure 14: stage III). The final stage of sulphide

precipitation is inferred to be cooler than initial stage I mineralisation (<280 ˚C) as chalcopyrite overgrowths are absent (Gill *et al.*, 2016; Safina *et al.*, 2016).

5.5 Paragenesis and Mechanisms of Se Enrichment

A mechanism for such a pronounced and temporary shift in hydrothermal fluid conditions needs to be addressed to explain the observed paragenesis. Magmatism is considered to be the ultimate driving force in VMS hydrothermal circulation (Choi and Lowell, 2015; Patten *et al.*, 2016). But the magmatic heat input into the hydrothermal system varies temporally as a function of magmatic flux. This was especially true in Troodos where spreading was accomplished by graben development and crustal thinning during periods of low magmatism (e.g. Varga and Moores, 1990). During periods of magmatic quiescence increased fault movement along graben bounding faults is predicted. Near surface fault movement could potentially increase permeability leading to seawater ingress into the upper VMS stratigraphy promoting a locally oxidising environment at Apliki. The South Apliki Breccia Zone is located between two faults with extensive rotation evident in both footwall and hanging wall lithologies, thus frequent fault movement seems likely. The mineralised contact is sharp with no clear indication of mineralisation outside the fault bound block (Figure 6). We infer that late slip on these bounding faults during the waning stages of VMS formation coupled with a reduced magmatic influx led to increased seawater ingress into the shallow hydrothermal system and locally oxidising neutral pH fluids temporarily promoted sulphide dissolution. The brecciated morphology of the South Apliki Breccia Zone supports this observation. Renewed magmatism and the sealing of permeability pathways due to mineral precipitation and possible magmatic volatile influx re-established reducing conditions and led to the formation of late stage III pyrite; a similar model is hypothesised for Ortaklar (see Yildirim *et al.*, 2016).

From textural analyses three stages of hypogene overprinting have been identified followed by a fourth stage of supergene alteration. Alteration stages based on geochemistry and mineralogy may be summarised as follows (see Figures 15 and 16):

Stage I: Chalcopyrite-pyrite mineralisation under reducing low pH <4, hypogene (>350 ˚C) fluids and the development of main stage VMS mineralisation under a constant magmatic-hydrothermal flux (Figure 10). Seawater Se/S ratios prevail averaging 330 (n=22) in pyrite; Se is sourced from epidosite zones +/- a minor magmatic component (Figure 13).

Stage II: Hematite mineralisation involving reduced hydrothermal input and ingress of seawater into the shallow hydrothermal system. Fluid with near neutral pH and increased fO_2 promotes sulphide dissolution and hematite formation. This phase is relatively short-lived given the modest alteration of chalcopyrite rims (Figure 8 and 9). Se/S values rapidly transition between seawater and magmatic dominant conditions averaging 2158 in pyrite (n=23) (Figure 13).

Stage III: Renewed magmatism and decreased fault movement limit further ingress of seawater and reducing conditions are re-established leading to the precipitation of euhedral pyrite overgrowths. Late chalcopyrite overgrowths are absent suggesting lower temperatures of formation (<280 ˚C) than stage I mineralisation. Se/S within Stage III pyrite is elevated averaging 3480 (n=22) indicating an increased magmatic component (Figure 13).

Stage IV represents supergene enrichment of chalcopyrite and pyrite. Samples span a wide range of Se/S ratios (28-3200) and contain significant amounts of covellite, chalcocite and digenite. Se/S ratios have not been determined for Cu secondaries but are likely to show a large amount of scatter due to the mobilisation of Se in low temperature fluids (Huston *et al.*, 1995).

5.6 The Extreme Enrichment of Se at the South Apliki Breccia Zone

We suggest that during the mature stages of VMS mineralisation the South Apliki Breccia Zone would have formed a high-temperature (>280 ˚C) stockwork overlain by massive sulphides. Stage I pyrite and chalcopyrite were formed under hot reduced conditions synonymous with VMS formation. In this period Se fractionated ‘normally’ and is preferentially enriched in chalcopyrite over pyrite. The transition to oxidising conditions and replacement of pyrite with hematite expelled

Se from the dissolving pyrite (Figures 15 and 16). LA-ICP-MS studies by Genna and Gaboury (2015) and qualitative TRA from this study show that Se cannot be accommodated in the crystal lattice of hematite in large concentrations. The dissolution of early stage I pyrite led to an excess of Se in solution. Stage III pyrite then precipitated under reducing conditions and due to the elevated concentration of Se in solution readily incorporated elements expelled from the dissolution of stage I pyrite (Figure 15). Te concentration remains constant in late pyrite as higher temperatures which favour Te incorporation (>280˚C) were absent during stage III mineralisation.

Theoretical data from Huston *et al.* (1995) shows that Se in pyrite decreases with increasing temperature from 700 ppm to <250 ppm as temperature increases from 150-300 ˚C (Huston *et al.*, 1995). Modelling also demonstrates that Se concentration in pyrite increases rapidly under oxidising conditions (log ($\Sigma SO_4/\Sigma H_2S$) >0) (~~refer back to~~ Figure 3). Based on this, stage III pyrite may have precipitated at temperatures as low as 150 ˚C at near neutral pH promoting the incorporation of Se into the crystal lattice. Higher temperatures of >300 ˚C are less favourable for Se Incorporation in pyrite with a theoretical maximum of 500 ppm Se; much less than the measured 1862 ppm average (n=23) (Figure 15 and 16). On this basis pyrite should be distinguishable on Se content which relates to temperature. At Apliki two generations of pyrite are clearly distinguishable based on Se content; stage I low Se high temperature pyrite (<250 ppm) and stage III pyrite that formed under cool <300 ˚C oxidised conditions containing >>250 ppm Se (Huston *et al.*, 1995) (see Figure 3).

The ability of Cu secondary minerals such as covellite to incorporate Se remains poorly characterised. Auclair *et al.* (1987) show that the Se content in chalcopyrite remains homogenous with increasing proportions of covellite and digenite. High concentrations of Se within Cu secondaries are reported for the Kidd Creek deposit (Hannington *et al.*, 1999); values for digenite average 0.44 wt.% with a maximum of 2.13 wt.% (Hannington *et al.*, 1999). It seems likely that Cu secondaries may host significant Se but further analyses are needed to accurately quantify the concentrations of Se in covellite and digenite.

The clear distinction in geochemistry between stage I and III pyrite suggests the timing of mineralisation is important in controlling Se enrichment. Se incorporation was not simply a function of redox; Se distribution between pyrite generations would be homogenous if this was true. Oxidising conditions present during the waning stage of VMS formation would have been short-lived and alone do not account for the observed enrichment in Se. In deposits such as Alestos (Troodos) a late pyrite overprint is absent and no enrichment in Se is recorded, however hematite is present, which indicates oxidised conditions. Instead we favour the mobilisation of Se from early stage I sulphides during the precipitation of hematite (Figure 15). The dissolution of Se from pyrite during hematite formation provides a mechanism explaining a) the distribution of Se and b) the extreme enrichment in late stage III pyrite.

6. Conclusion

The South Apliki Breccia Zone is both mineralogically and geochemically distinct within the Solea graben and the Troodos ophiolite. It is significantly enriched in Se with maximum values of 4953 ppm in pyrite and 3956 ppm in chalcopyrite, which are greater than any previously known values for sulphides in Cyprus-type VMS. Dissolution of sulphides and precipitation of oxides caused by an influx of seawater due to fault movement and decreased magmatic-hydrothermal input led to fluctuations in fO_2 from reduced to oxidising conditions. Se/S ratios suggest an initially seawater dominated system transitioning to magmatic in stage III pyrite. The addition of a late magmatic input is proposed as a mechanism to restore reducing conditions necessary for stage III pyrite formation. Conditions of stage III mineralisation were cooler (<280 ˚C) than stage I mineralisation promoting Se incorporation into pyrite. Hematite does not have the same ability as pyrite to accommodate large volumes of Se within its crystal lattice and so the dissolution of early sulphide minerals and precipitation of oxides left an excess of Se in solution. A final magmatic influx toward the end of VMS formation led to overprinting of oxidised facies with late stage euhedral pyrite. This late stage III pyrite acted as a sink for excess Se and is enriched up to 4953 ppm (averaging 1862 ppm, n=23). By

comparison stage I pyrite, which was not affected by Se displaced during earlier hematite formation averages 182 ppm Se (n =22). This paper highlights the possible significance of varied redox, dissolution and reprecipitation in achieving high levels of Se enrichment in VMS systems. The findings of this study indicate that chalcopyrite possesses a greater affinity for Se over Te and that rarely, under specific conditions the uptake of Se in chalcopyrite can be matched or be exceeded by pyrite. This study suggests that deposits with fluctuating redox and late oxidising overprints may contain appreciable Se; moreover this could be important in terms of additional by-product resources and assessing the environmental impact of mining.

Acknowledgments

This research was supported by the Natural Environmental Research Council (NERC) under the tellurium and selenium cycling and supply grant NE/L002191/1 and NE/M010848/1. We thank the Geological Survey Department (GSD) of Cyprus for kindly supplying regional soil geochemistry data. A special thank you to Dr. Andreas Zissimos and the Director Dr. Costas Constantinou for their continued support and enthusiasm. We also thank Hellenic Copper Mines for allowing access to the Apliki mine and Dr. Michael Green, Iphigenia Gabriel and Lazaros Georgiou for their support and advice in the field. We acknowledge the input of Prof. Gawen Jenkin and Dr. Manuel Keith at Leicester University, their guidance helped greatly in advancing this publication. Thanks to Dr. Brian O'Driscoll and an anonymous reviewer for their comments which greatly improved the clarity of this manuscript. This publication is dedicated to the late Prof. Hazel Prichard. Without Hazel none of the above would have been possible, her infectious enthusiasm and passion for geology remain an inspiration.

Supplementary material

To view supplementary material for this article, please visit https://doi.org/xxxxxxxxx

6. References

Adamides, N. (2011). Mafic-dominated volcanogenic sulphide deposits in the Troodos ophiolite, Cyprus Part 1- The deposits of the Solea graben. *Applied Earth Science*. **119**, 65–77.

Adamides, N. (2010). Mafic-dominated volcanogeneic sulphide deposits in the Troodos ophiolite, Cyprus Part 2- A review of genetic models and guides for exploration. *Applied Earth Science*. **119**, 193–204.

Auclair, G., Fouquet, Y. and Bohn, M. (1987). Distribution of selenium in high temperature hydrothermal sulfide deposits at 13 degrees north, East Pacific Rise. *Canadian Mineralogist*. **25**, 577–587.

Barrie, M.D.H. (1999). Classification of Volcanic-Associated Massive Sulfide Deposits Based on Host-Rock Composition. *Reviews in Economic Geology*. **8**, 1–11.

Bendnarz, U. and Schmincke, H.-U. (1990). Chemical patterns of seawater and hydrothermal alteration in the northeastern Troodos extrusive series and the sheeted dyke complex (Cyprus). Pp 639-654 in: *OPHIOLITES Oceanic Crustal Analogues* (Malpas, J., Moores, E.M., Panayiotou, A. and Xenophontos, C. eds.) Troodos 87 Ophiolites and Oceanic Lithosphere, Geological Survey Department of Cyprus, Nicosia, Cyprus.

Bickle, M.J. and Teagle, D.A.H. (1992). Strontium alteration in the Troodos ophiolite: implications for fluid fluxes and geochemical transport in mid-ocean ridge hydrothermal systems. *Earth and Planetary Science Letters*. **113**, 219–237.

Bustamante, M.L. and Gaustad, G. (2014). The Evolving Copper-Tellurium Byproduct System: A Review of Changing Production Techniques & Their Implications. Pp 11-16. in: *Rare Metal Technology 2014*. (Neelameggham, N.R., Alam, S., Oosterhof, H., Jha, A., Wang, S. eds.). The Minerals, Metals & Materials Society, 143rd Annual Meeting, John Wiley & Sons, UK.

Butler, I.B. and Nesbitt, R.W. (1999). Trace element distributions in the chalcopyrite wall of a black smoker chimney: insights from laser ablation inductively coupled plasma mass spectrometry (LA–ICP–MS). *Earth and Planetary Science Letters*. **167**, 335–345.

Chen, M., Campbell, I.H., Xue, Y., Tian, W., Ireland, T.R., Holden, P., Cas, R.A.F., Hayman, P.C. and Das, R. (2015). Multiple Sulfur Isotope Analyses Support a Magmatic Model for the Volcanogenic Massive Sulfide Deposits of the Teutonic Bore Volcanic Complex, Yilgarn Craton, Western Australia. *Economic Geology*. **110**, 1411–1423.

Choi, J. and Lowell, R.P. (2015). The response of two-phase hydrothermal systems to changing magmatic heat input at mid-ocean ridges. *Deep Sea Research*. Part II Topical Studies in Oceanography, Exploring New Frontiers in Deep-Sea Research: In Honor and Memory of Peter A. Rona**. 121**, 17–30.

Cohen, D.R., Rutherford, N.F., Morisseau, E. and Zissimos, A.M. (2012). Geochemical patterns in the soils of Cyprus. *Science of the Total Environment*. **420**, 250–262.

Cox, D. and Singer, D.A. (1986). Mineral Deposit Models- US Geological Survey Bulletin 1693, 1st ed, US Geological Survey Bulletin. U.S Geological Survey.

Doyle, M.G. and Allen, R.L. (2003). Subsea-floor replacement in volcanic-hosted massive sulfide deposits. *Ore Geology Reviews*. **23**, 183–222.

Economou-Eliopoulos, M., Eliopoulos, D.G. and Chryssoulis, S. (2008). A comparison of high-Au massive sulfide ores hosted in ophiolite complexes of the Balkan Peninsula with modern analogues: Genetic significance. *Ore Geology Reviews.* **33**, 81–100.

Eddy, C.A., Dilek, Y., Hurst, S. and Moores, E.M. (1998). Seamount formation and associated caldera complex and hydrothermal mineralization in ancient oceanic crust, Troodos ophiolite (Cyprus). *Tectonophysics.* **292**, 189–210.

Escartín, J. and Canales, J.-P. (2011). Detachments in oceanic lithosphere: deformation, magmatism, fluid flow and ecosystems. EOS, *Transactions AGU* (92). **4**, 25 January 2011.

Franklin, J.M., Gibson, H.L., Jonasson, I.R. and Galley, A.G. 2005. Volcanogenic Massive Sulfide Deposits. P.p 523-560. In: *Economic Geology 100th Anniversary Volume* (Hedenquist, J.W., Thompson, J.F.H., Goldfarb, R.J., and Richards, J.P., eds.), Society of Economic Geologists

Galley, A., Hannington, M. and Jonasson, I., 2007. Volcanogenic Massive Sulphide Deposits. Pp. 141-161. In: *Mineral Deposits of Canada: A Synthesis of Major Deposit-Types, District Metallogeny, the Evolution of Geological Provinces, and Exploration Methods.* (W.D. Goodfellow, ed.), Geological Association of Canada, Special Publication, No. 5.

Gass, I. G. (1968). Is the Troodos Massif of Cyprus a Fragment of Mesozoic Ocean Floor? *Nature.* **220** (5162), pp. 39-42.

Gass, I.G. (1980). The Troodos massif: Its role in the unravelling of the ophiolite problem and its significance in the understanding of constructive plate margin processes. Pp. 23-35. in: *Ophiolites, Proceedings: International Ophiolite Symposium, Cyprus 1979* (A. Panayiotou ed.). The Geological Survey Department, Nicosia, Cyprus.

Gass, I.G., MacLeod, C.J., Murton, B.J., Panayiotou, A., Simonian, K.O. and Xenophontos, C. (1994). The Geological Evolution of the Southern Troodos Transform Fault Zone .Pp 218. in: Cyprus Geological Survey Memoir 9, Geological Survey Department, Nicosia, Cyprus

Genna, D. and Gaboury, D. (2015). Deciphering the Hydrothermal Evolution of a VMS System by LA-ICP-MS Using Trace Elements in Pyrite: An Example from the Bracemac-McLeod Deposits, Abitibi, Canada, and Implications for Exploration. *Economic Geology*. **110**, 2087–2108.

Gill, S.B., Piercey, S.J. and Layton-Matthews, D. (2016). Mineralogy and Metal Zoning of the Cambrian Zn-Pb-Cu-Ag-Au Lemarchant Volcanogenic Massive Sulfide (VMS) Deposit, Newfoundland. *Canadian Mineralogist*. **54**, 1307–1344.

Gillis, K.M. and Roberts, M.D. (1999). Cracking at the magma–hydrothermal transition: evidence from the Troodos Ophiolite, Cyprus. *Earth and Planetary Science Letters*. **169**, 227–244. -4

Gillis, K.M. and Robinson, P.T. (1990). Patterns and processes of alteration in the lavas and dykes of the Troodos Ophiolite, Cyprus. *Journal of Geophysical Research*. **95**, 21523–21548.

Gillis, K.M. and Robinson, P.T. (1980). Multistage alteration in the extruisve sequence of the Troodos ophiolite, Cyprus. Pp. 655-664 in: *OPHIOLITES Oceanic Crustal Analogues* (Malpas, J., Moores, E.M., Panayiotou, A. and Xenophontos, C. eds.) Troodos 87 Ophiolites and Oceanic Lithosphere, Geological Survey Department of Cyprus, Nicosia, Cyprus.

Graham, S.D., Holwell, D.A., McDonald, I., Jenkin, G.R.T., Hill, N.J., Boyce, A.J., Smith, J. and Sangster, C. (2017). Magmatic Cu-Ni-PGE-Au sulfide mineralisation in alkaline igneous systems: An example from the Sron Garbh intrusion, Tyndrum, Scotland. *Ore Geology Reviews*. **80**, 961–984.

Grundler, P.V., Brugger, J., Etschmann, B.E., Helm, L., Liu, W., Spry, P.G., Tian, Y., Testemale, D. and Pring, A. (2013). Speciation of aqueous tellurium(IV) in hydrothermal solutions and vapors, and the role of oxidized tellurium species in Te transport and gold deposition. *Geochimica et Cosmochimica Acta*. **120**, 298–325.

Hannington, M.D., Galley, A., Herzig, P. and Petersen, S. (1998). Comparison of the TAG mound and stockwork complex with Cyprus-type massive sulfide deposits. Pp. 389-415. in: *Ocean Drilling Program Scientific Results* (Herzig, P.M., Humphris, S.E., Miller, D.J. and Zierenberg, R.A. eds.). College Station, Texas (Ocean Drilling Program).

Hannington, M.D. and Barrie, C.T. (1999). The giant Kidd Creek volcanogenic massive sulfide deposit: Western Abitibi Subprovince, Canada. *Economic Geology*. **10**, 1-11

Herzig, P.M., Hannington, M.D. and Arribas A. Jr (1998). Sulfur isotopic composition of hydrothermal precipitates from the Lau back-arc: implications for magmatic contributions to seafloor hydrothermal systems. *Mineralium Deposita.* **33**, 226–237.

Holwell, D.A., Keays, R.R., McDonald, I. and Williams, M.R. (2015). Extreme enrichment of Se, Te, PGE and Au in Cu sulfide microdroplets: evidence from LA-ICP-MS analysis of sulfides in the Skaergaard Intrusion, east Greenland. *Contributions to Mineralogy and Petrology*. **170**, 1–26.

Humphris, S.E. and Cann, J.R. (2000). Constraints on the energy and chemical balances of the modern TAG and ancient Cyprus seafloor sulfide deposits. *Journal of Geophysical Research*. **105**, 28477–28488.

Huston, D.L. and Large, R.R. (1989). A chemical model for the concentration of gold in volcanogenic massive sulphide deposits. *Ore Geology Review*s. **4**, 171–200.

Huston, D.L., Sie, S.H. and Suter, G.F. (1995). Selenium and its importance to the study of ore genesis: the theoretical basis and its application to volcanic-hosted massive sulfide deposits using pixeprobe analysis. *Nuclear Instruments and Methods in Physics Research Section B: Beam Interactions with Materials and Atoms*. **104**, 476–480.

Jowitt, S.M., Jenkin, G.R.T., Coogan, L.A. and Naden, J. (2012). Quantifying the release of base metals from source rocks for volcanogenic massive sulfide deposits: Effects of protolith composition and alteration mineralogy. *Journal of Geochemical Exploration*. **118**, 47–59.

Jowitt, S.M., Osborn, R.G.M., Thomas, R.D.H., Naden, J., Gunn, A.G., Herrington, R.J. and Nicolaides, S. (2005). 'T'-type mineralisation — a pseudo-epithermal style of VHMS associated gold mineralisation, Cyprus. *Mineral Deposit Research: Meeting the Global Challenge*. 635–637.

Keith, M., Haase, K.M., Klemd, R., Krumm, S. and Strauss, H. (2016). Systematic variations of trace element and sulfur isotope compositions in pyrite with stratigraphic depth in the Skouriotissa volcanic-hosted massive sulfide deposit, Troodos ophiolite, Cyprus. *Chemical Geology*. **423**, 7-18

Layton-Matthews, D., Leybourne, M.I., Peter, J.M., Scott, S.D., Cousens, B. and Eglington, B.M. (2013). Multiple sources of selenium in ancient seafloor hydrothermal systems: Compositional and Se, S, and Pb isotopic evidence from volcanic-hosted and volcanic-sediment-hosted massive sulfide deposits of the Finlayson Lake District, Yukon, Canada. *Geochimica et Cosmochimica Acta*. **117**, 313–331.

Layton-Matthews, D., Peter, J.M., Scott, S.D. and Leybourne, M.I. (2008). Distribution, Mineralogy, and Geochemistry of Selenium in Felsic Volcanic-Hosted Massive Sulfide Deposits of the Finlayson Lake District, Yukon Territory, Canada. *Economic Geology*. **103**, 61–88.

Lu, D., Chang, Y., Yang, H. and Xie, F. (2015). Sequential removal of selenium and tellurium from copper anode slime with high nickel content. *Transactions of Nonferrous Metal Society of China.* **25**, 1307–1314.

Maslennikov, V.V., Maslennikova, S.P., Large, R.R. and Danyushevsky, L.V. (2009). Study of Trace Element Zonation in Vent Chimneys from the Silurian Yaman-Kasy Volcanic-Hosted Massive Sulfide Deposit (Southern Urals, Russia) Using Laser Ablation-Inductively Coupled Plasma Mass Spectrometry (LA-ICPMS). *Economic Geology*. **104**, 1111–1141.

Melekestseva, I.Y., Maslennikov, V.V., Tret'yakov, G.A., Nimis, P., Beltenev, V.E., Rozhdestvenskaya, I.I., Maslennikova, S.P., Belogub, E.V., Danyushevsky, L., Large, R., Yuminov, A.M. and Sadykov, S.A. (2017). Gold- and Silver-Rich Massive Sulfides from the Semenov-2 Hydrothermal Field, 13°31.13'N, Mid-Atlantic Ridge: A Case of Magmatic Contribution? *Economic Geology*. **112**, 741–773.

Miyashiro, A. (1973). The Troodos Ophiolitic Complex was probably formed in an island arc. *Earth and Planetary Sciene Letters.* **19**, 218-224.

Moss, R.L., Tzimas, E., Kara, H., Willis, P. and Kooroshy, J. (2013). The potential risks from metals bottlenecks to the deployment of Strategic Energy Technologies. *Energy Policy, Special section: Long Run Transitions to Sustainable Economic Structures in the European Union and Beyond*. **55**, 556–564.

Nuriel, P., Katzir, Y., Abelson, M., Valley, J.W., Matthews, A., Spicuzza, M.J. and Ayalon, A. (2009). Fault-related oceanic serpentinization in the Troodos ophiolite, Cyprus: implications for a fossil oceanic core complex. *Earth and Planetary Science Letters*, **282**, 34-4.

Patten, C.G.C., Pitcairn, I.K., Teagle, D.A.H. and Harris, M. (2016). Mobility of Au and related elements during the hydrothermal alteration of the oceanic crust: implications for the sources of metals in VMS deposits. *Mineralium Deposita*. **51**, 179–200.

Patten, C.G.C., Pitcairn, I.K. and Teagle, D.A.H. (2017). Hydrothermal mobilisation of Au and other metals in supra-subduction oceanic crust: Insights from the Troodos ophiolite. *Ore Geology Reviews*. **86**, 487–508.

Pearce, J.A., Lippard, S.J., and Roberts, S. (1984). Characteristics and tectonic significance of supra-subduction zone ophiolites. Pp. 77-96. In*: Ophiolites and Oceanic Lithosphere* (Gass, I.G., Lippard, S.J. and Shelton, A.W. eds.). Geological Society of London, No. 13

Pearce, J.A. and Robinson, P.T. (2010). The Troodos ophiolitic complex probably formed in a subduction initiation, slab edge setting. *Gondwana Research*, A Tribute to Miyashiro. **18**, 60–81.

Perkins, W.T. (2011). Extreme selenium and tellurium contamination in soils — An eighty year-old industrial legacy surrounding a Ni refinery in the Swansea Valley. *Science of the Total Environment*. **412–413**, 162–169.

Prichard, H.M., Knight, R.D., Fisher, P.C., McDonald, I., Zhou, M.-F. and Wang, C.Y. (2013). Distribution of platinum-group elements in magmatic and altered ores in the Jinchuan intrusion, China: an example of selenium remobilization by postmagmatic fluids. *Mineralium Deposita*. **48**, 767–786.

Rahm, M., Hoffmann, R. and Ashcroft, N.W. (2016). Atomic and Ionic Radii of Elements 1–96. *Chemistry – A European Journa*l. **22**, 14625–14632.

Rautenschlein, M., Jenner, G.A., Hertogen, J., Hofmann, A.W., Kerrich, R., Schmincke, H.-U. and White, W.M. (1985). Isotopic and trace element composition of volcanic glasses from the Akaki Canyon, Cyprus: implications for the origin of the Troodos ophiolite. *Earth and Planetary Science Letters*. **75**, 369–383.

Revan, M.K., Genç, Y., Maslennikov, V.V., Maslennikova, S.P., Large, R.R. and Danyushevsky, L.V. (2014). Mineralogy and trace-element geochemistry of sulfide minerals in hydrothermal chimneys from the Upper-Cretaceous VMS deposits of the eastern Pontide orogenic belt (NE Turkey). *Ore Geology Reviews*. **63**, 129–149.

Richardson, C.J., Cann, J.R., Richards, H.G. and Cowan, J.G. (1987). Metal-depleted root zones of the Troodos ore-forming hydrothermal systems, Cyprus. *Earth and Planetary Science Letters*, 84, 243–253.

Robertson, A. and Xenophontos, C. (1993). Development of concepts concerning the Troodos ophiolite and adjacent units in Cyprus. *Geological Society of London Special Publication*. **76**, 85–119.

Robertson, A.H.F. (2002). Overview of the genesis and emplacement of Mesozoic ophiolites in the Eastern Mediterranean Tethyan region. *Lithos*. **65**, 1–67.

Robinson, P.T., Melson, W.G., O'Hearn, T. and Schmincke, H.-U. (1983), Volcanic glass compositions of the Troodos ophiolite, Cyprus. Geology. 11, 400-404.

Robinson, P. and Malpas, J. (1987). The Troodos ophiolite of Cyprus: New perspectives on its origin and emplacement. Pp. 13-26 in: *OPHIOLITES Oceanic Crustal Analogues* (Malpas, J., Moores, E.M., Panayiotou, A. and Xenophontos, C. eds.) Troodos 87 Ophiolites and Oceanic Lithosphere, Geological Survey Department of Cyprus, Nicosia, Cyprus.

Safina, N.P., Melekestseva, I.Y., Nimis, P., Ankusheva, N.N., Yuminov, A.M., Kotlyarov, V.A. and Sadykov, S.A. (2016). Barite from the Saf'yanovka VMS deposit (Central Urals) and Semenov-1 and Semenov-3 hydrothermal sulfide fields (Mid-Atlantic Ridge): a comparative analysis of formation conditions. *Mineralium Deposita*. **51**, 491–507.

Schiffman, P., Bettison, L.A. and Smith, B. (1990). Epidosites of the Solea graben. Pp 673-684 in: *OPHIOLITES Oceanic Crustal Analogues* (Malpas, J., Moores, E.M., Panayiotou, A. and Xenophontos, C. eds.) Troodos 87 Ophiolites and Oceanic Lithosphere, Geological Survey Department of Cyprus, Nicosia, Cyprus.

Seyfried, W. and Bischoff, J.L. (1977). Hydrothermal transport of heavy metals by seawater: The role of seawater/basalt ratio. *Earth and Planetary Science Letters*. **34**, 71–77.

Seyfried, W.E. Jr. and Mottl, M.J. (1982). Hydrothermal alteration of basalt by seawater under seawater-dominated conditions. *Geochimica at Cosmochimica Acta*. **46**, 985–1002.

Sillitoe, R.H., Hannington, M.D. and Thompson, J.F.H. (1996). High sulfidation deposits in the volcanogenic massive sulfide environment. *Economic Geology*. **91**, 204–212.

Smith, J.W., Holwell, D.A., McDonald, I. and Boyce, A.J. (2016). The application of S isotopes and S/Se ratios in determining ore-forming processes of magmatic Ni–Cu–PGE sulfide deposits: A cautionary case study from the northern Bushveld Complex. *Ore Geology Reviews*. **73**, Part 1, 148–174.

Tornos, F., 2006. Environment of formation and styles of volcanogenic massive sulfides: The Iberian Pyrite Belt. *Ore Geology Reviews*. **28**, 259–307.

Tornos, F., Peter, J.M., Allen, R. and Conde, C. (2015). Controls on the siting and style of volcanogenic massive sulphide deposits. *Ore Geology Reviews*. **68**, 142–163.

Varga, R.J. (1991). Modes of extension at oceanic spreading centres: evidence from the Solea graben, Troodos ophiolite, Cyprus. *Journal of Structural Geology*. **13**, 517–537.

Varga, R.J. and Moores, E.M. (1990). Intermittent magmatic spreading and tectonic extension in the Troodos Ophiolite: implications for exploration for black smoker-type ore deposits. Pp. 53-64 in: *OPHIOLITES Oceanic Crustal Analogues* (Malpas, J., Moores,, E.M., Panayiotu, A. and Xenophontos, C. eds.) Troodos 87 Ophiolites and Oceanic Lithosphere, Geological Survey Department of Cyprus, Nicosia, Cyprus.

Varga, R.J. and Moores, E.M. (1985). Spreading structure of the Troodos ophiolite, Cyprus. *Geology*. **13**, 846–850.

Vibetti, N.J. (1993). Chemical alteration trends, fluid inclusion patterns and stable isotope compositions in the plutonic sequence of the Troodos ophiolite, Cyprus. *Journal of African Earth Sciences*. Middle East. **17**, 193–202.

Yamaoka, K., Matsukura, S., Ishikawa, T. and Kawahata, H. (2015). Boron isotope systematics of a fossil hydrothermal system from the Troodos ophiolite, Cyprus: Water–rock interactions in the oceanic crust and subseafloor ore deposits. *Chemical Geology*. **396**, 61–73.

Yildirim, N., Dönmez, C., Kang, J., Lee, I., Pirajno, F., Yıldırım, E., Günay, K., Seo, J.H., Farquhar, J. and Chang, S.W., (2016). A magnetite-rich Cyprus-type VMS deposit in Ortaklar: A unique VMS style in the Tethyan metallogenic belt, Gaziantep, Turkey. *Ore Geology Reviews*. **79**, 425–442.

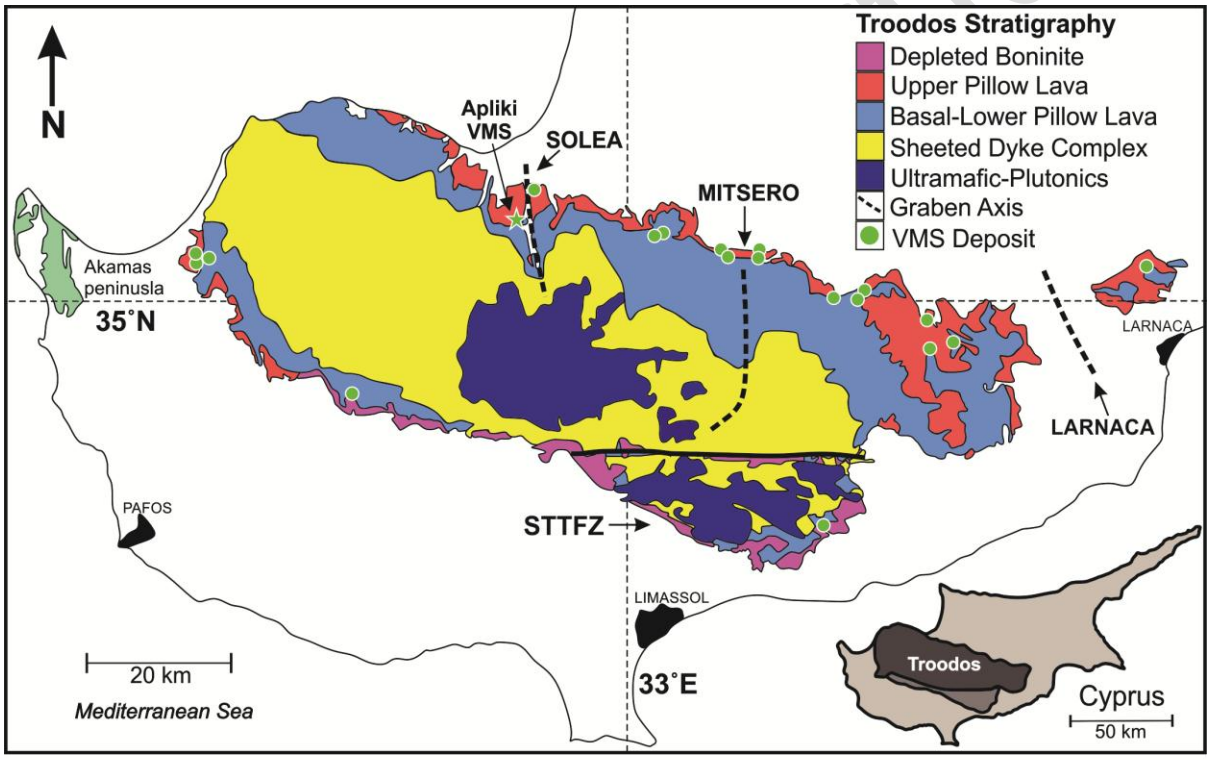

Figure 1A: Simplified geological map of Troodos

Figure 1A:

Simplified geological map of the late Cretaceous (92 Ma) Troodos ophiolite, Cyprus. Apliki VMS is located in NW Troodos, W of the Solea graben axis (adapted from Keith *et al*., 2016).

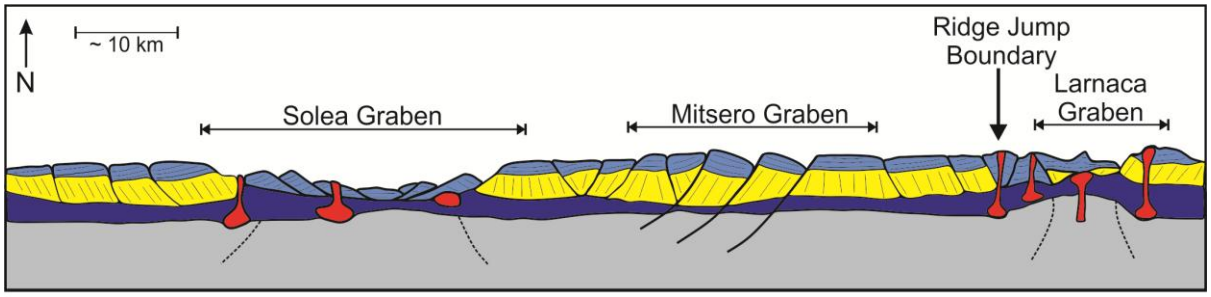

Figure 1B: Schematic cross section of north Troodos

Figure 1B:

Simplified structural cross-section of Troodos. Normal fault rotation leads to inversely dipping dykes and lava stratigraphy. VMS form along faults related to three main grabens: Solea, Mitsero and Larnaca. Location of section corresponds to the north flank of Troodos (adapted from Varga and Moores, 1990).

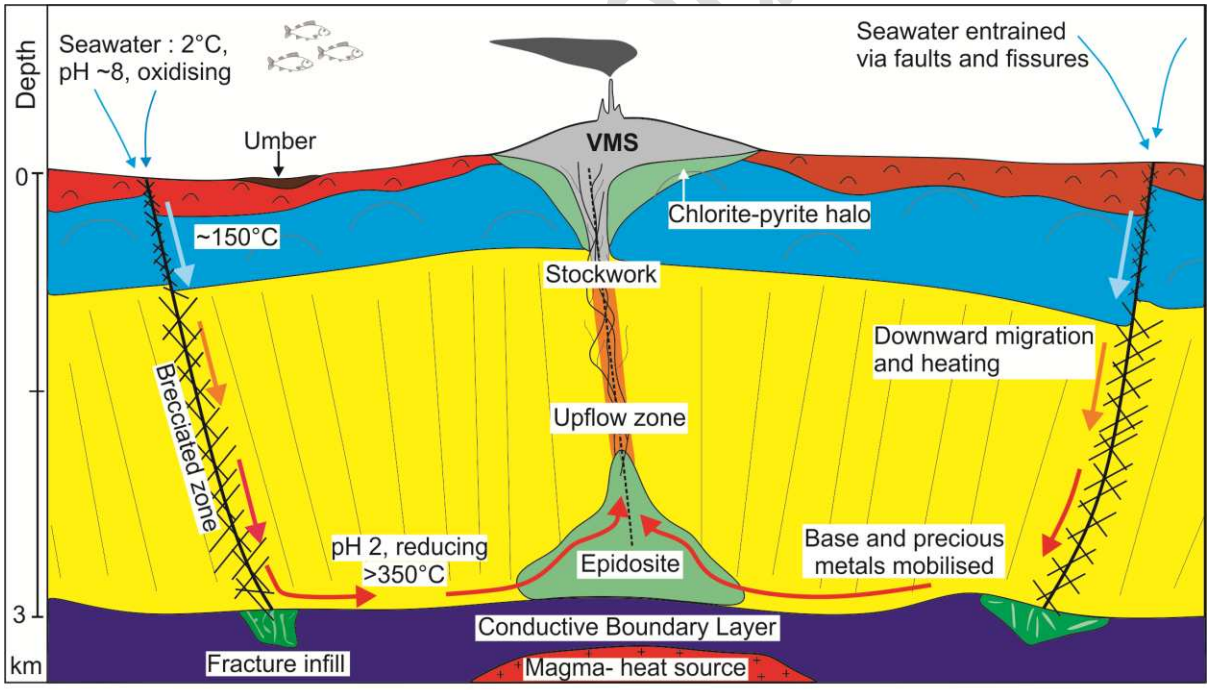

Figure 2: The VMS hydrothermal system

Figure 2:

Schematic section of the VMS hydrothermal system. Entrained seawater migrates downwards through the lava pile to the SDC. Fluid becomes superheated at the base of SDC forming epidosites.

Thermally buoyant evolved fluid rises through faults and is exhaled at the seafloor forming VMS deposits (adapted from Bickle and Teagle, 1992).

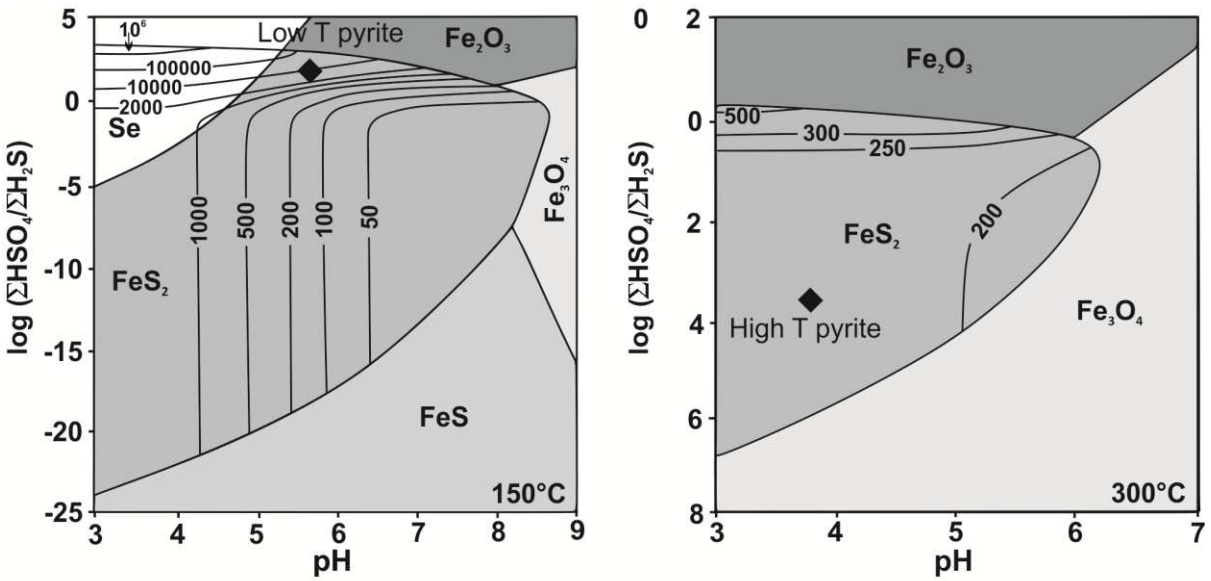

Figure 3: Thermodynamic modelling of Se in pyrite

Figure 3:

Theoretical incorporation of Se in pyrite as a function of pH, Eh and temperature. Se incorporation favours low temperatures and low pH (left). Se is enriched at low temperatures (left - 150 ˚C) over high temperatures in pyrite (right - 300 ˚C). Values are in ppm and S=0.002 m for both experiments (adapted from Huston *et al*., 1995).

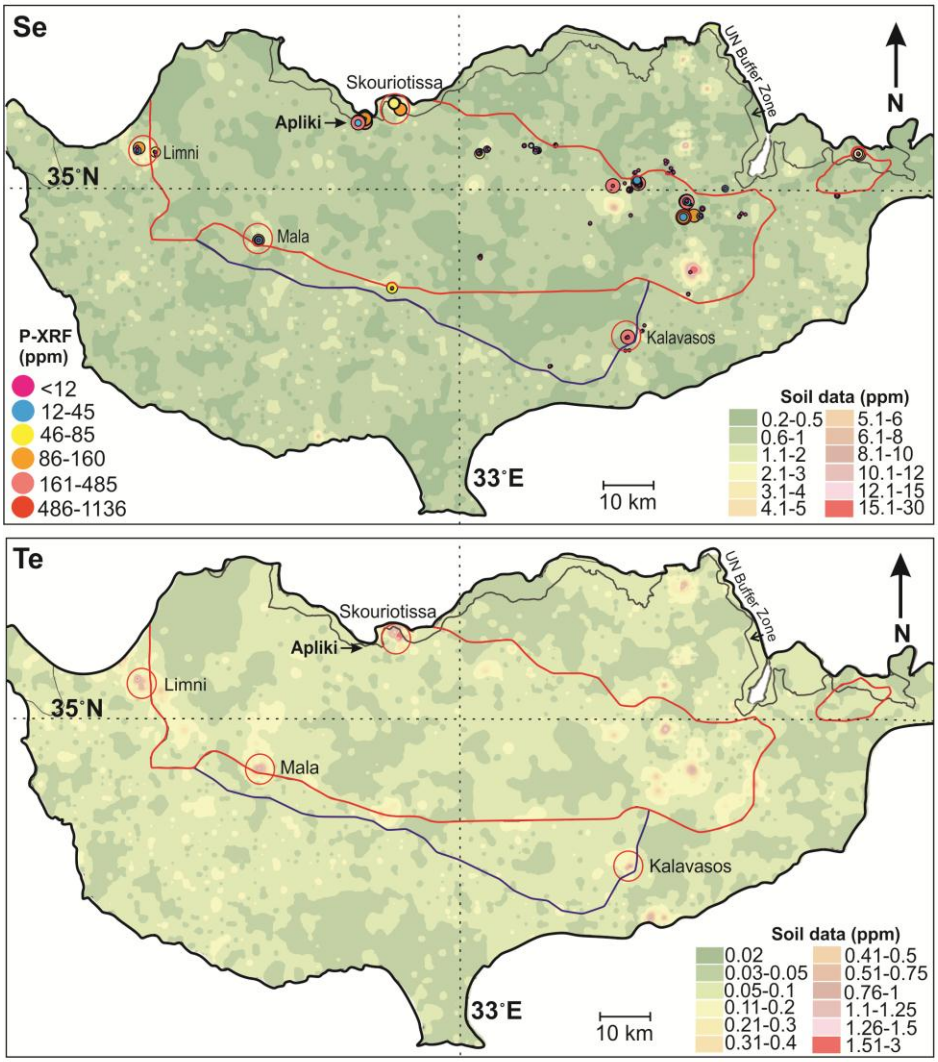

Figure 4: Te and Se Soil regional geochemistry, Transect A (0-25 cm)

Figure 4:

Distribution of Te and Se within soils in southern Cyprus. Two sets of data are presented for Se. P-XRF (this study) and regional geochemical soil data (Cohen *et al.,* 2012). Te was not analysed by P-XRF. The red line is the outline of the Troodos ophiolite and blue line the STTFZ. Anomalous Te and Se occur at the VMS mines; four of which are highlighted by the red circles. Data provided by the Geological Survey Department of Cyprus (after Cohen *et al*., 2012).

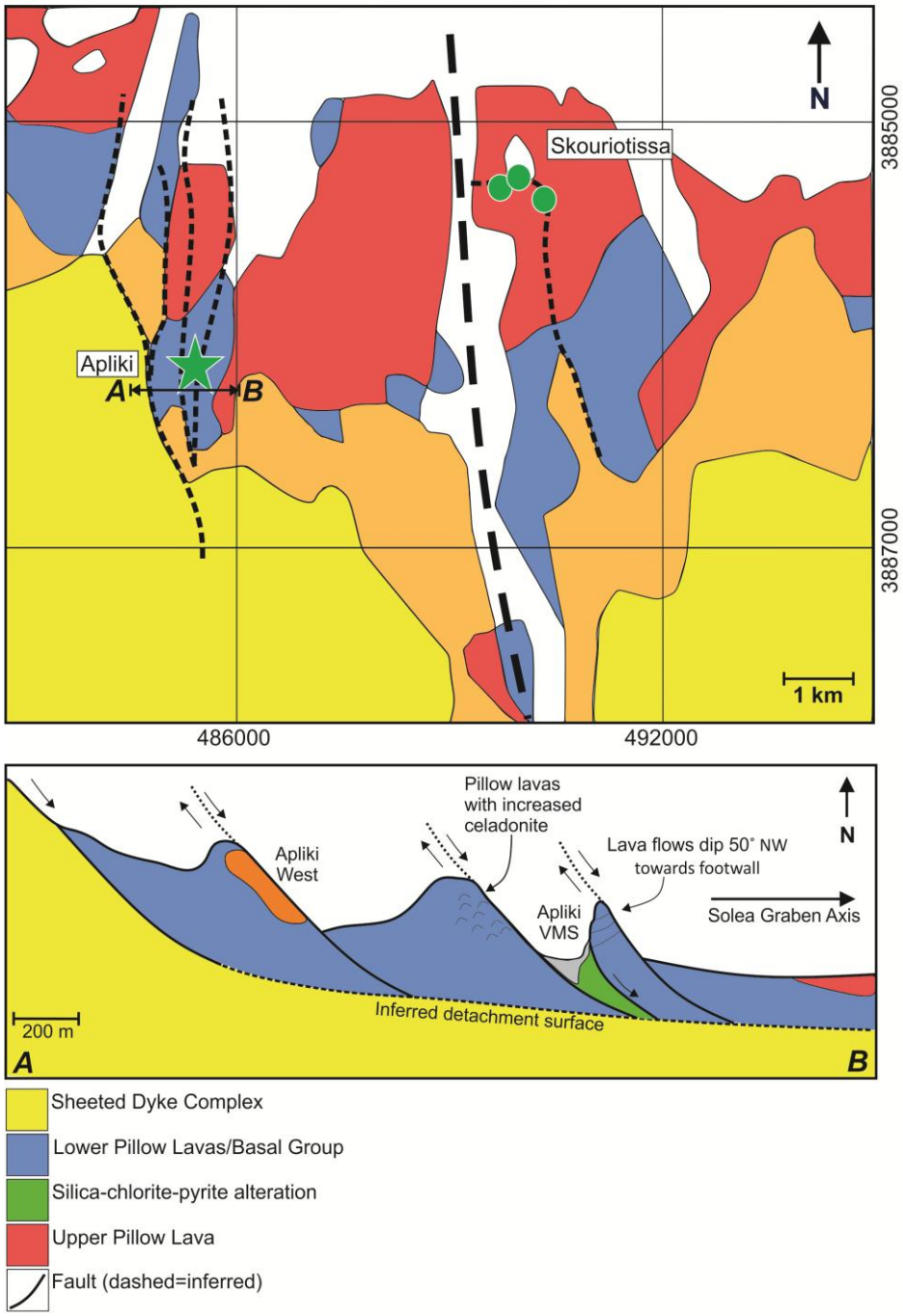

Figure 5A: Local geology of Solea Graben and schematic cross-section of Apliki VMS

Figure 5A:

Location map of the Apliki VMS and structural schematic cross-section. Apliki is located in NW Troodos within the Solea graben. The deposit is situated within the LPL stratigraphy and bound by two axis parallel (N-S) normal faults. At depth faults are inferred to truncate along a major detachment surface (Data from field mapping and GSD 1:250,000 map).

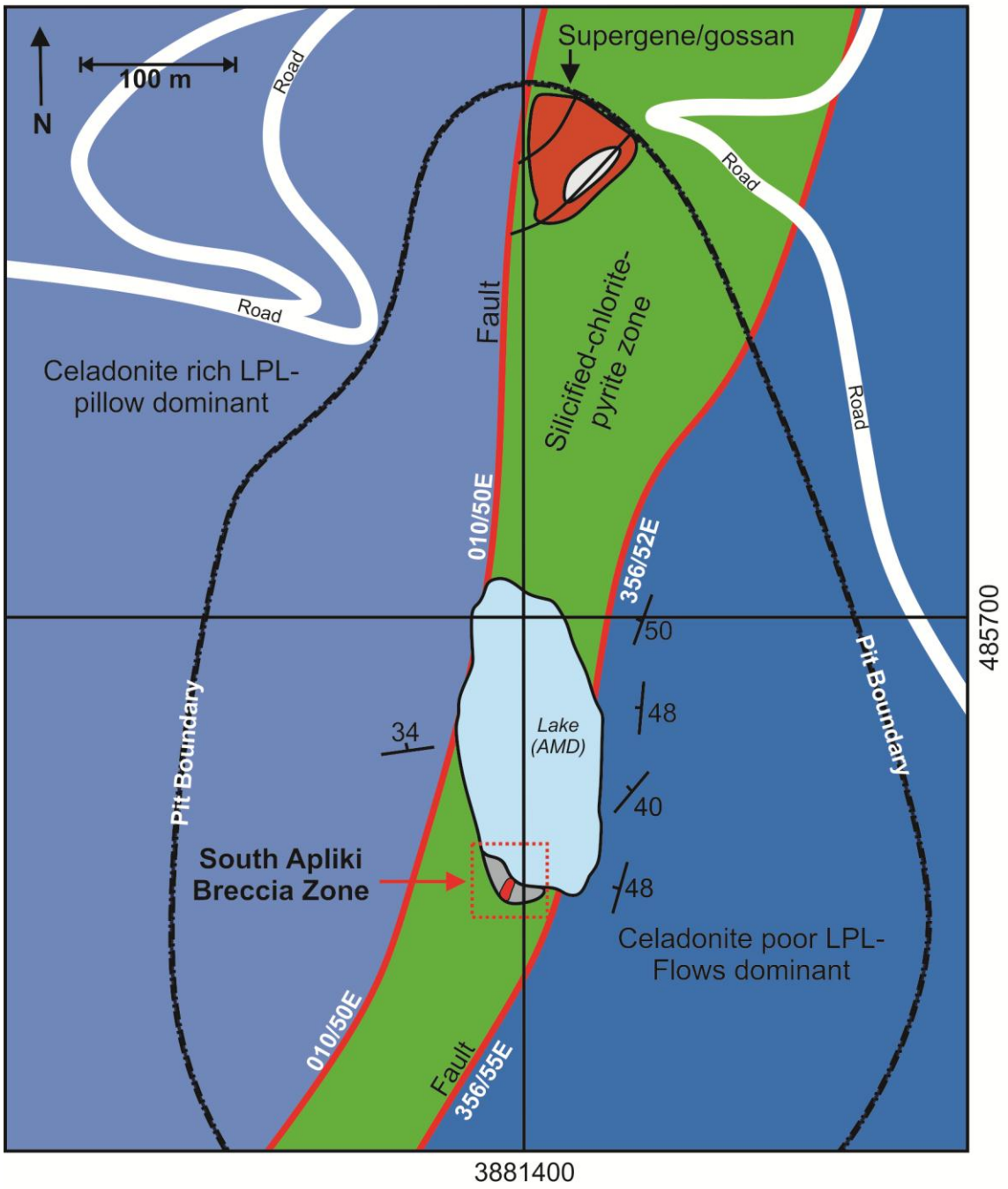

Figure 5B: Local geology map of Apliki

Figure 5B:

Local map of the Apliki showing the location of the South Apliki Breccia Zone and major geological features visible within the pit.

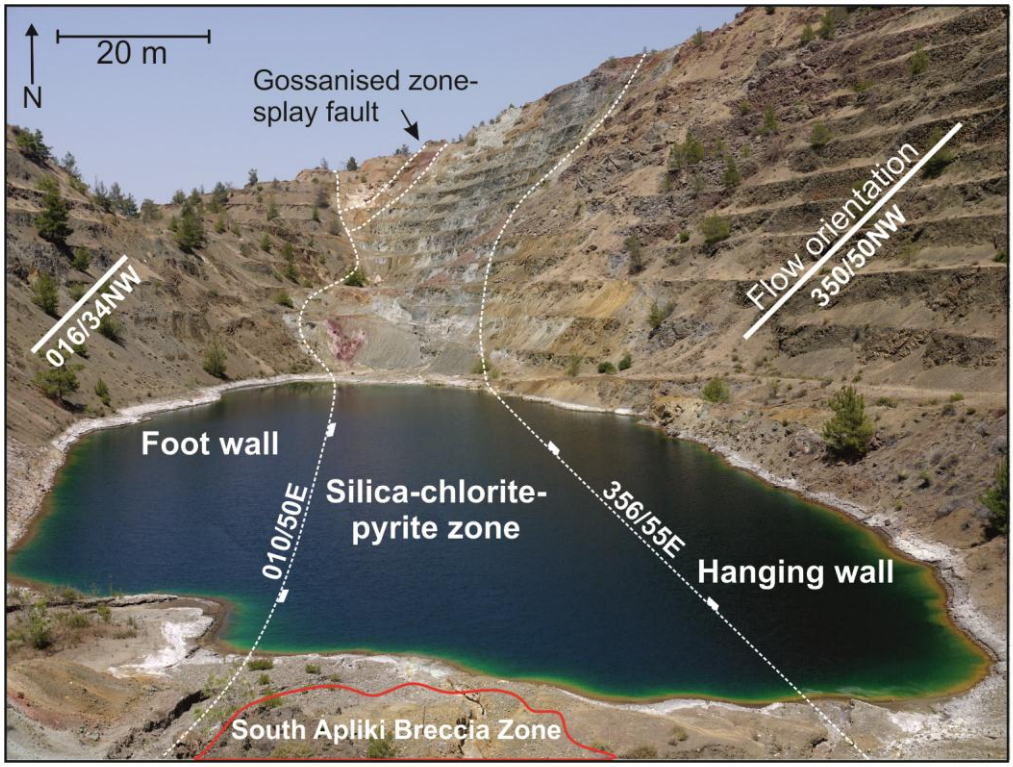

Figure 6: Annotated photo of Apliki open pit

Figure 6:

Annotated field photo of the Apliki VMS open pit. N-S faults bound the mineralised package, both the footwall and hanging wall are steeply rotated suggesting Apliki has undergone rotation off axis.

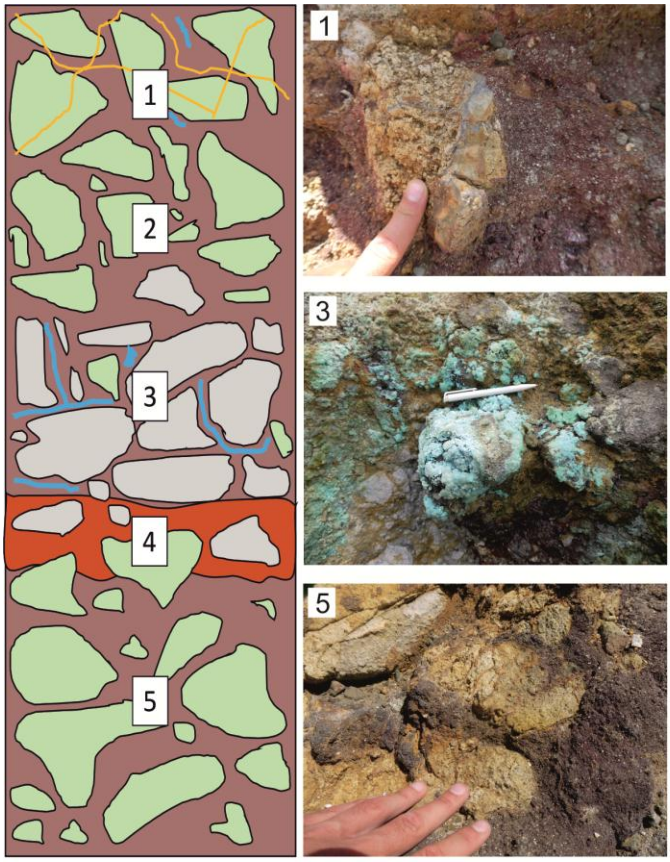

Zone 1: Upper zone. Well developed hematite matrix with euhedral fine grained <1mm pyrite. Breccia is matrix supported with 10-30 cm chloritised wall rock fragments. Goethite and azurite present in late veins.

Zone 2: Highly angular clasts of chloritised wall rock with hematite matrix. Chalcopyrite and covellite common (>15%) with euhedral pyrite. Goethite is absent.

Zone 3: Semi-massive ore. Subhedral pyrite increases to >40%. Hematite is less common forming 1-2 cm veins, breccia is clast supported. Azurite and chalcanthite common.

Zone 4: Jasper horizon. Fresh euhedral pyrite readily observed in matrix supported semi-silicified hematite. Chalcopyrite is minor <15%.

Zone 5: Hematite dominant zone. Matrix is well developed with abundant chalcopyrite (>20%) and pyrite (>30%). Clasts of wall rock are silicified with disseminated pyrite.

Figure 7: Cross-section of the South Apliki Breccia Zone

Figure 7:

Stratigraphic cross-section through the South Apliki Breccia Zone (see Table 1).

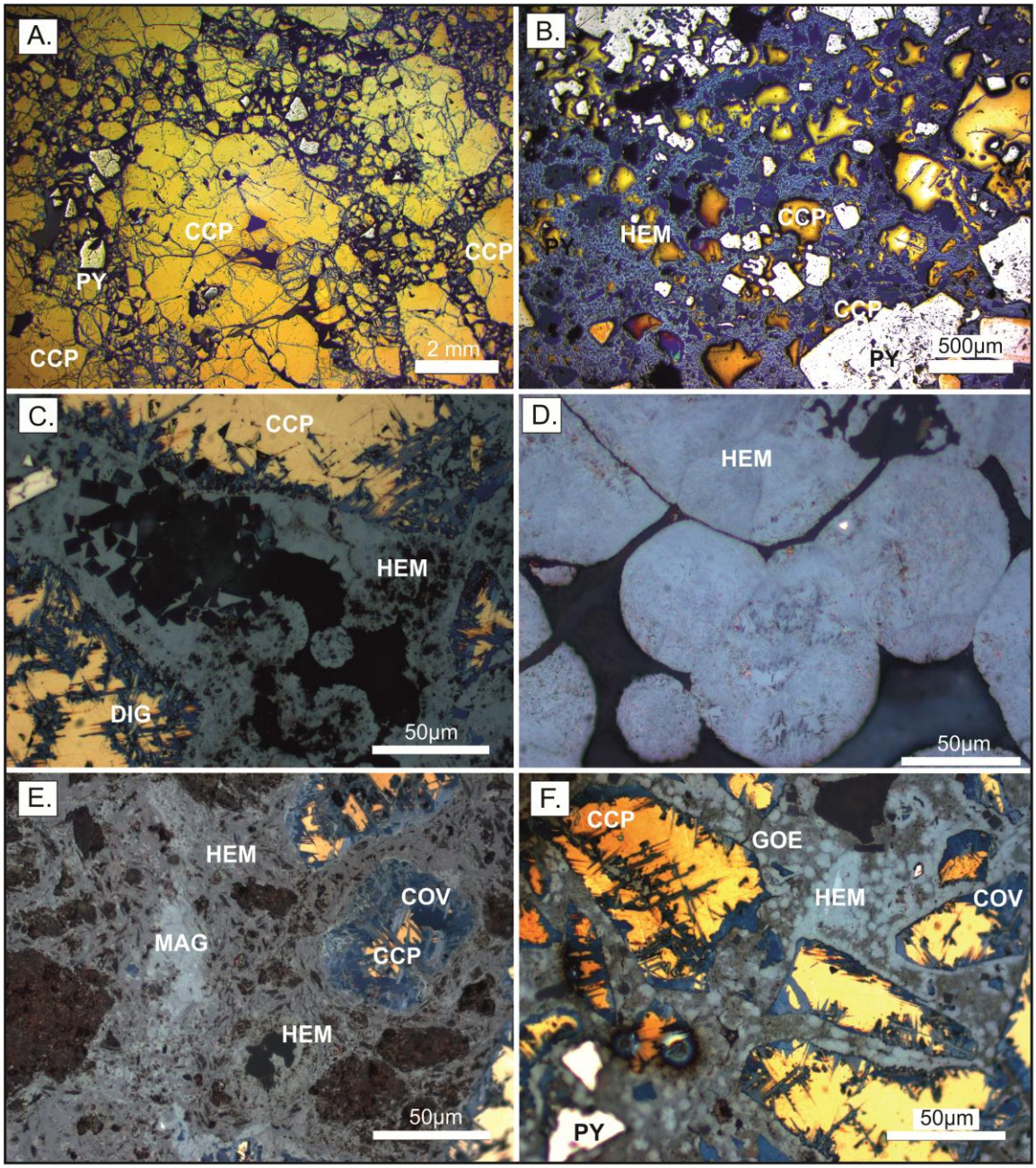

Figure 8: Reflected light photomicrographs from the Southern Apliki Breccia Zone

Figure 8:

Photomicrographs in reflected light of South Apliki Breccia Zone samples. A) Massive chalcopyrite with interstitial subhedral pyrite and minor covellite. B) Chalcopyrite with a hematite matrix and euhedral pyrite overgrowths. C) Chalcopyrite rimed by covellite and digenite with cubic hematite pseudomorphing pyrite. D) Botryoidal hematite with pyrite inclusions (white). E) Extensive alteration of pyrite to hematite with covellite replacing chalcopyrite. F) Botryoidal matrix hematite-goethite with subhedral pyrite and chalcopyrite rimmed by covellite. PY= pyrite CCP= chalcopyrite HEM= hematite COV= covellite DIG= digenite MAG= magnetite GOE= goethite

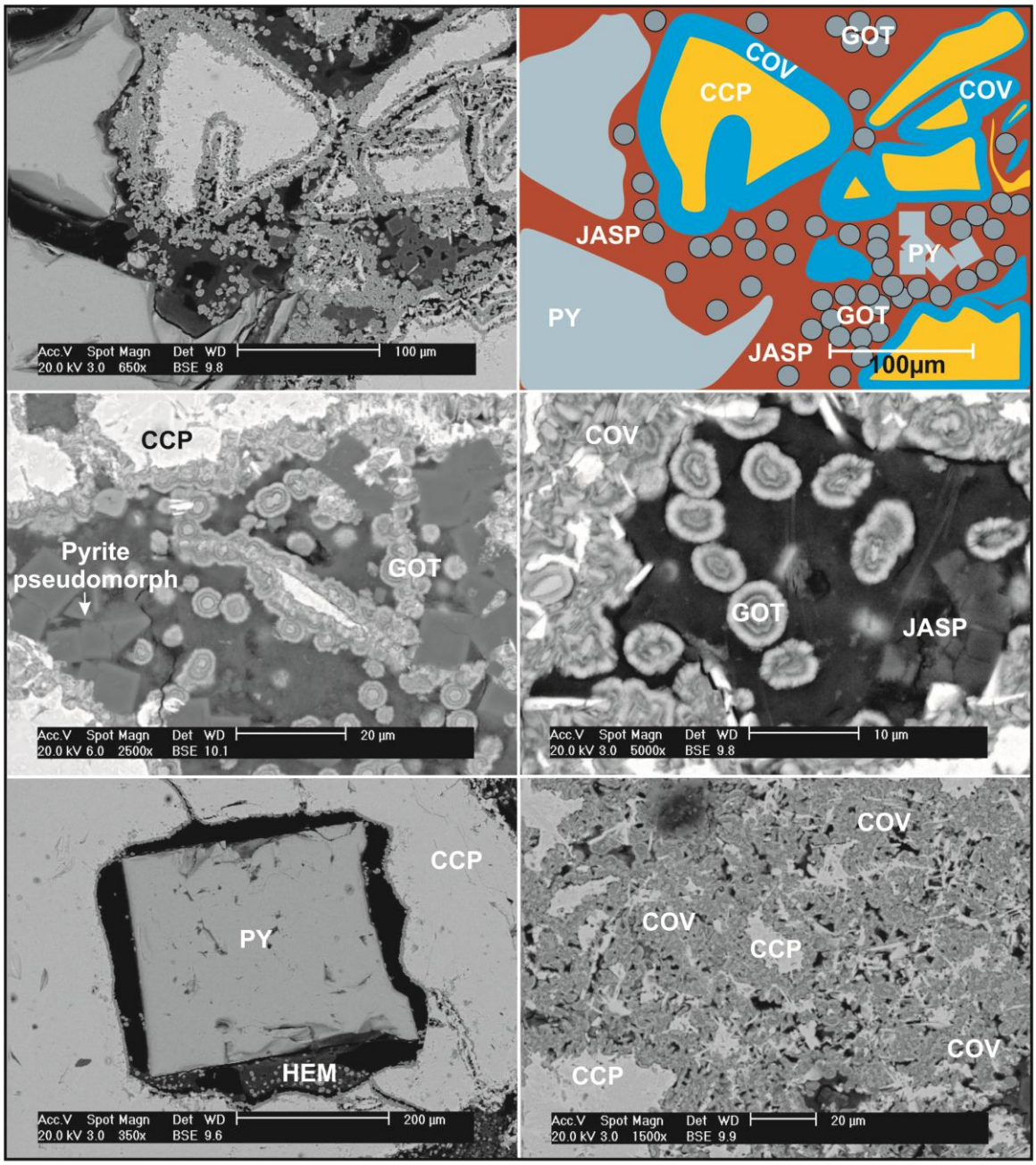

Figure 9: SEM BSE images

Figure 9:

SEM BSE photomicrographs. A) Oxidation of chalcopyrite rims to secondary Cu phases and botryoidal goethite in jasper. B) Sketch showing alteration of CCP. C) Pyrite pseudomorphs and goethite in matrix. D) Botryoidal goethite within jasper matrix. E) Euhedral pyrite within chalcopyrite and minor hematite at margins. F) Extensive alteration of chalcopyrite to covellite. PY= pyrite CCP= chalcopyrite HEM= hematite COV= covellite GOT= goethite JASP= Jasper (hematite + silica).

Figure 10: Sample Paragenesis

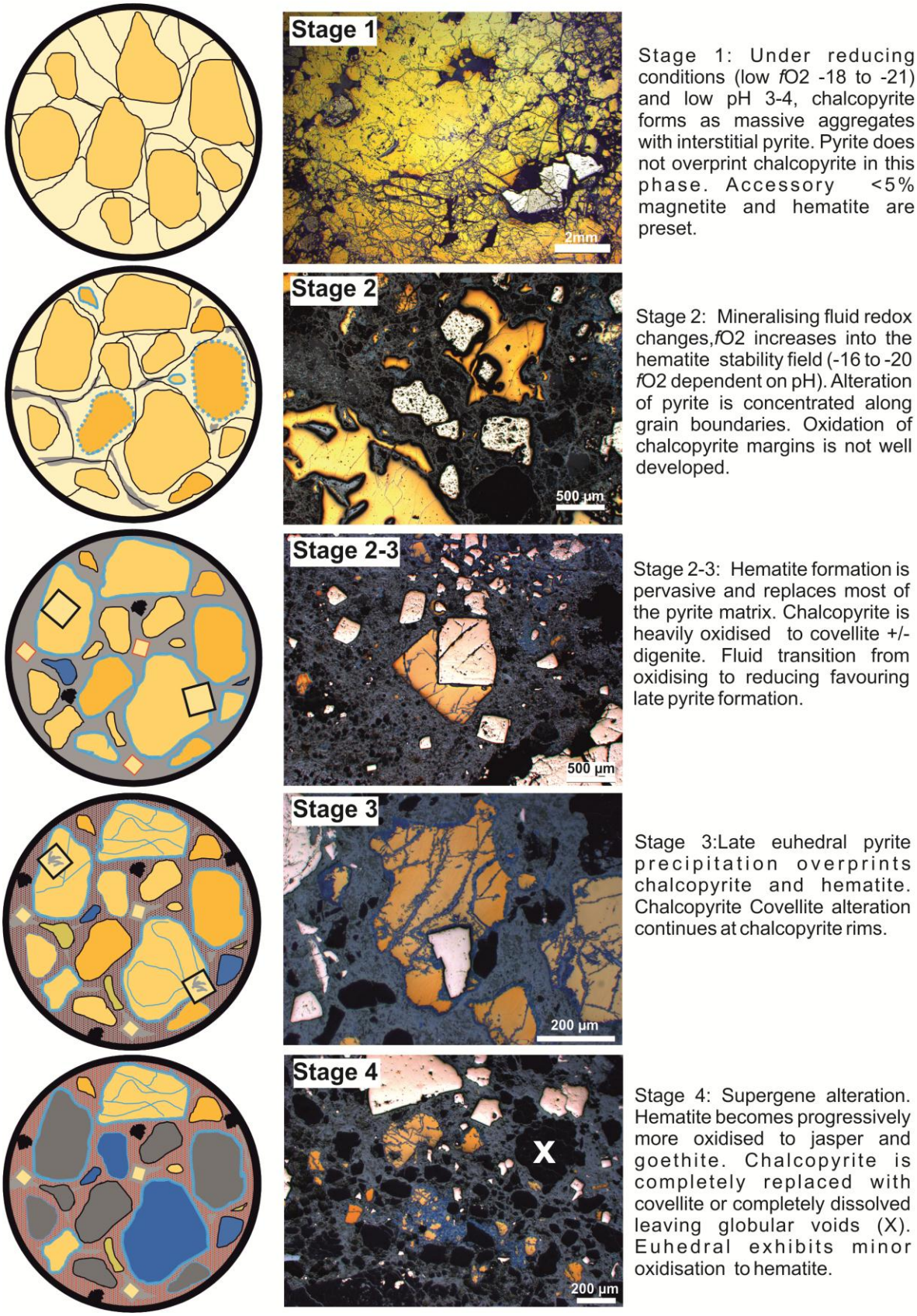

Figure 10:

Paragenesis of the South Apliki Breccia Zone

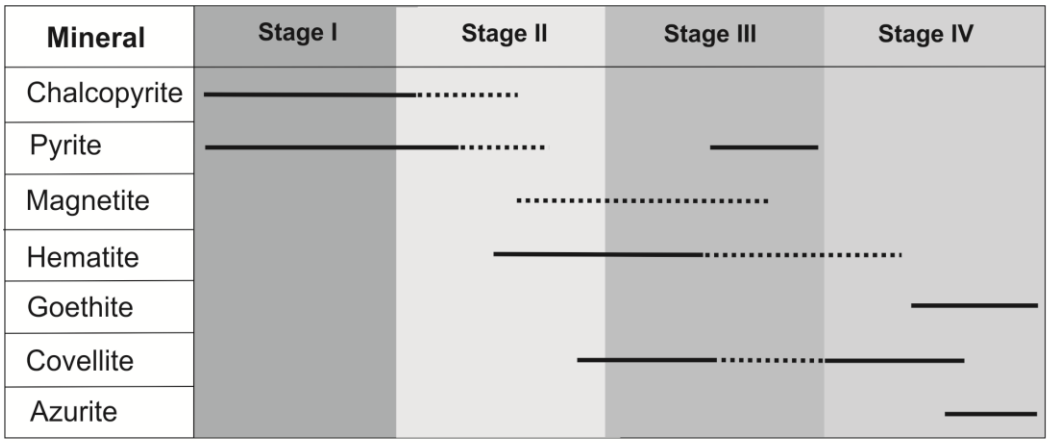

Figure 11: Summary of sample paragenesis

Figure 11:

Summary of sample paragenesis showing multiple phases of pyrite formation and the transition from sulphide to oxide formation. Goethite and chalcanthite are related to weathering and supergene alteration.

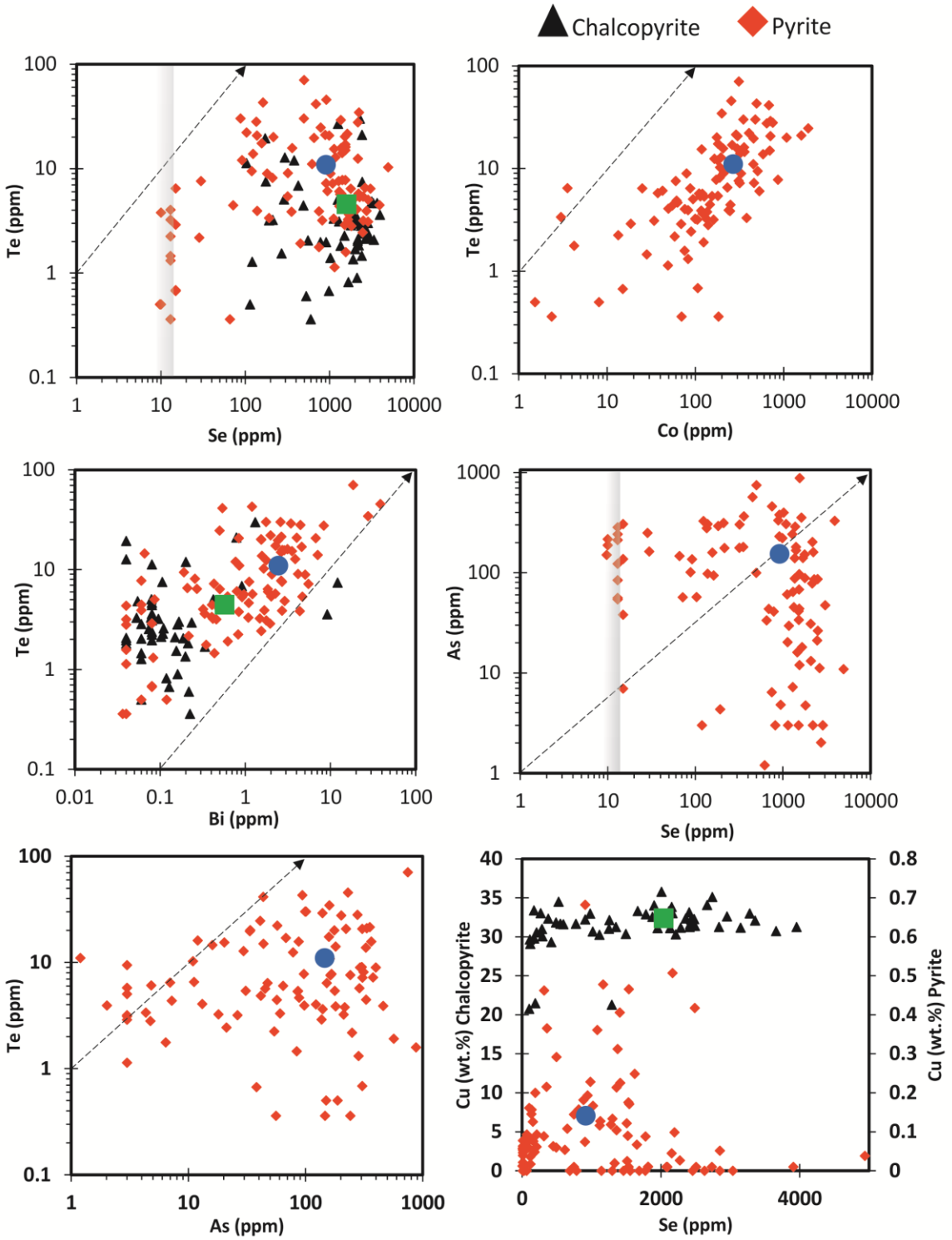

Figure 12: Bivariate plots. LA-ICP-MS of pyrite and chalcopyrite

Figure 12:

Bivariate plots of LA-ICP-MS spot analyses. Grey box indicates variable detection limit. Blue circle is average concentration for pyrite, green triangle for chalcopyrite (ppm).

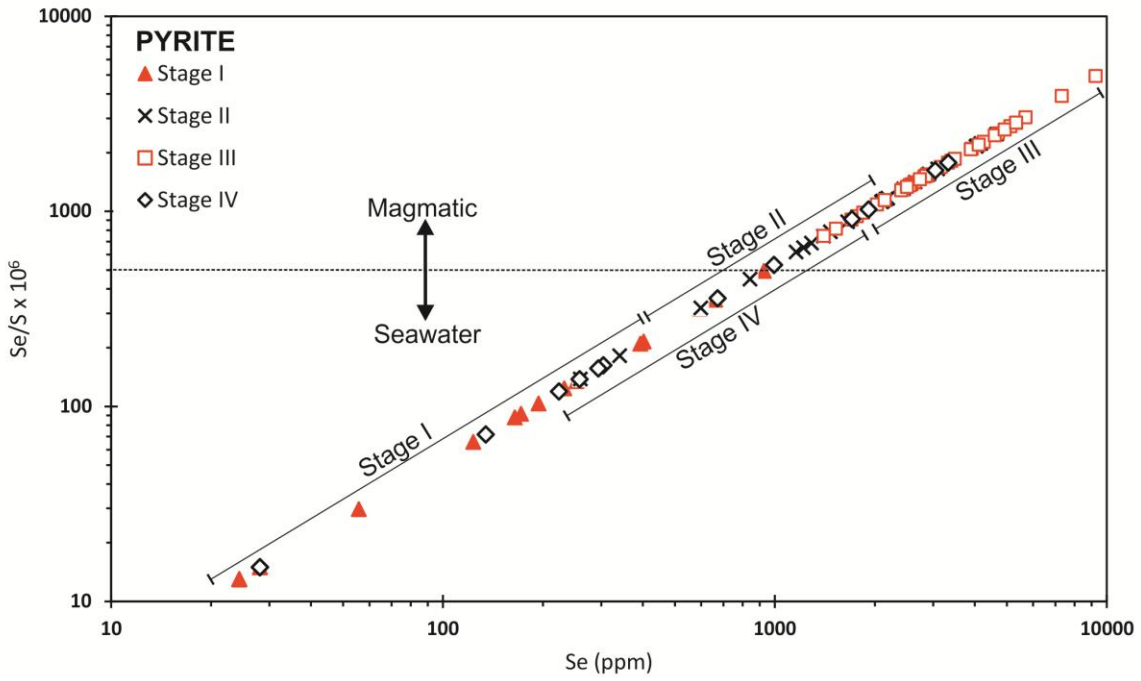

Figure 13: Se/S ratios vs. Se with alteration stage

Figure 13:

Se/S ratios vs. Se (ppm) for the South Apliki Breccia Zone. Se/S ratios in pyrite increase from alteration stages I-III. Stage IV (supergene) is highly variable. S is estimated at a stoichiometric value of 53.5 % for pyrite.

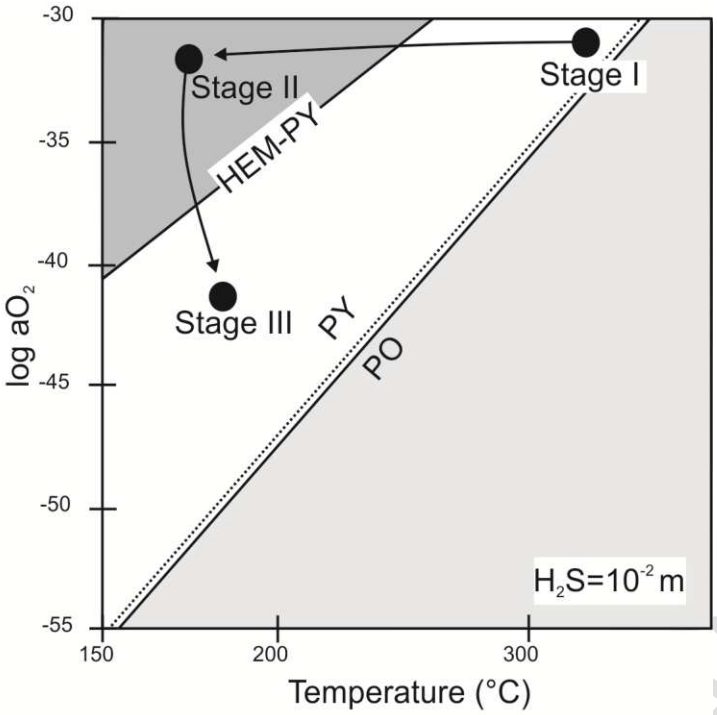

Figure 14: aO_2-temperature plot

Figure 14:

Stability field for pyrrhotite (PO), pyrite (PY) and hematite (HEM) in log aO_2 and temperature space. Stage I, II and III refer to sample paragenesis from reducing to oxidising and then returning to reducing, low temperature conditions at the South Apliki Breccia Zone (adapted from Layton-Matthews *et al*., 2008)

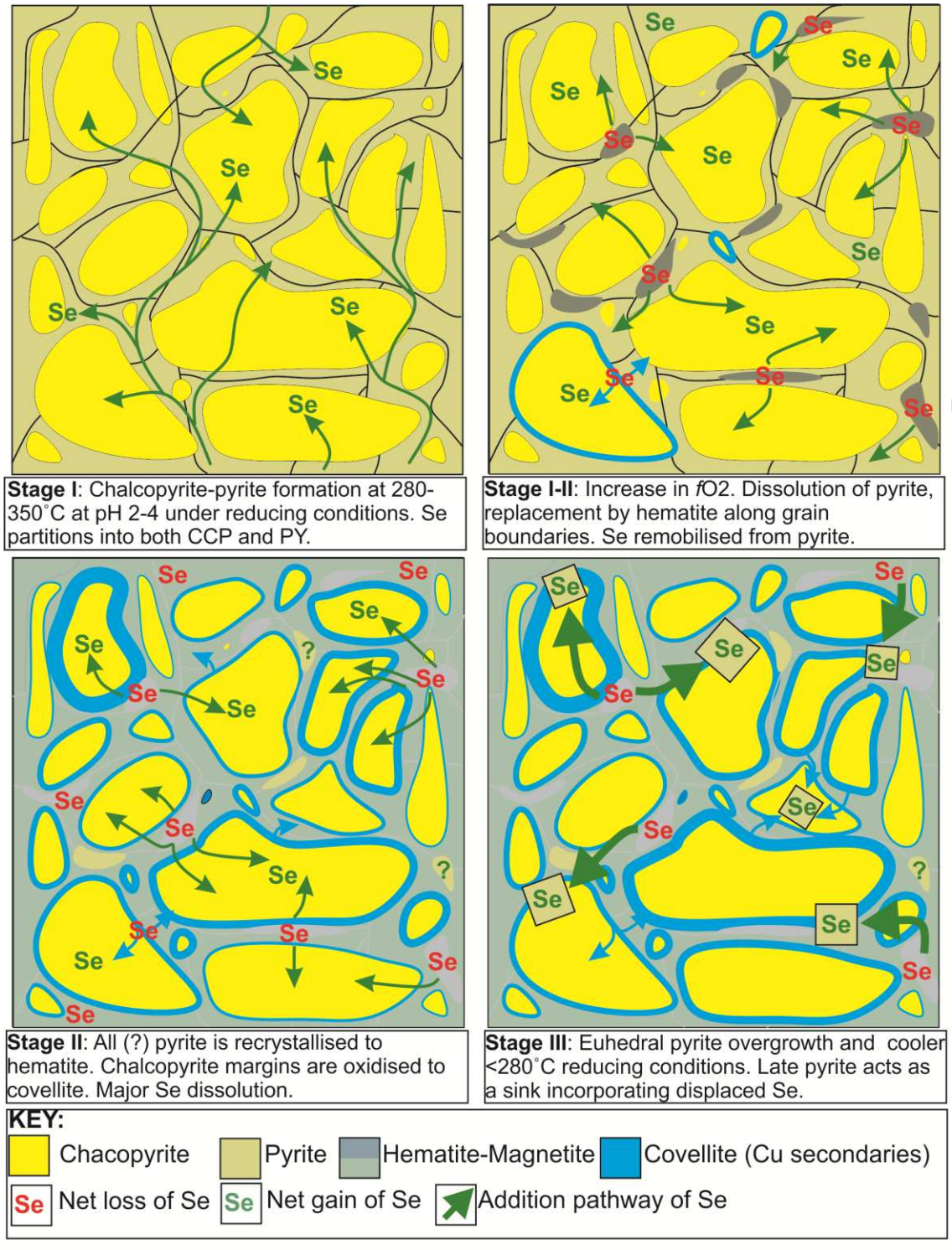

Figure 15: The extreme enrichment of Se

Figure 15:

Summary schematic for the extreme enrichment of Se at the South Apliki Breccia Zone.

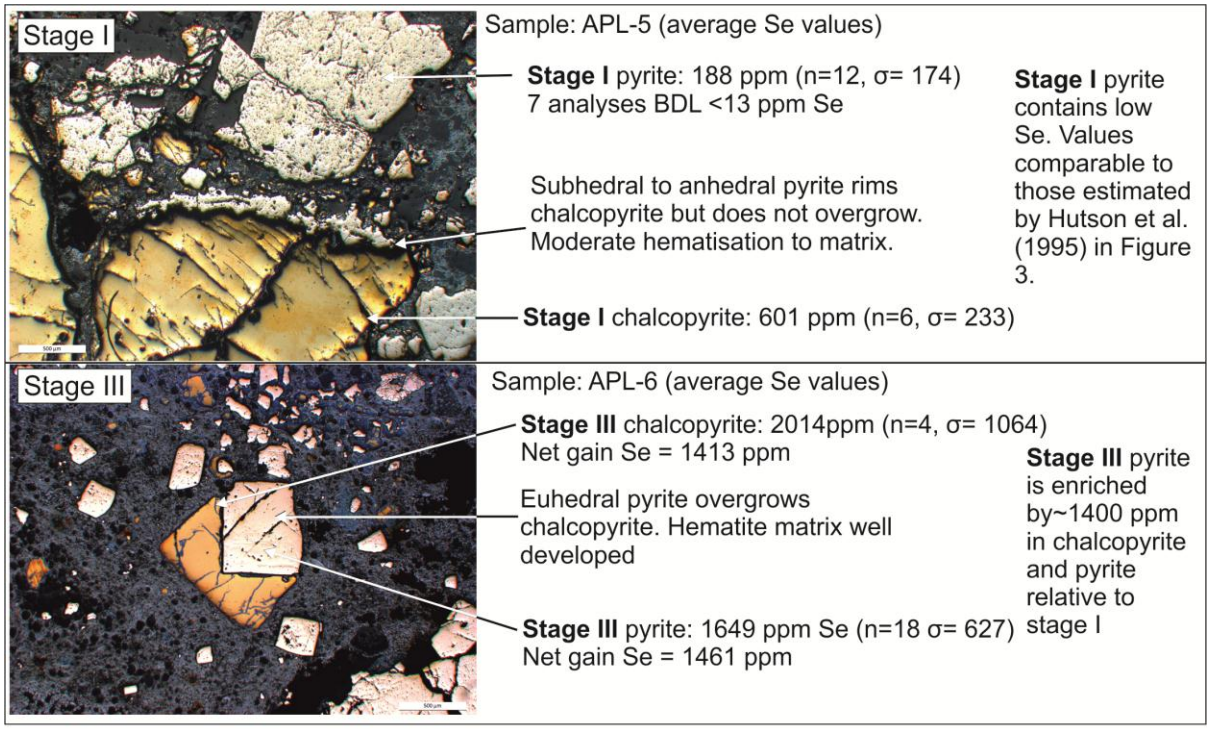

Figure 16: Geochemistry of end member stage I-III samples

Figure 16:

Geochemical comparison of stage I and III pyrite and chalcopyrite. Data is highly variable but demonstrates a net gain in Se of ~1400 ppm between stage I and III pyrite.

Table 1:

Summary of samples analysed from the South Apliki Breccia Zone. BDL= Below Detection Limit. σ = one standard deviation (in ppm) - full dataset available in Appendix.

Table 1:

Sample	Grid Reference (WGS 1950)	Stage	Mineralogy	Average Se PY (ppm)	Average Te PY (ppm)	Average Se CCP (ppm)	Average Te CCP (ppm)
APL-1	048574 3881375	3	Chalcopyrite (65%), covellite (20%), hematite (10%), pyrite (5%)	2075 (n=5) (σ =1080)	5.3 (n=5) (σ = 3.3)	2648 (n=10) (σ = 745)	3.5 (n=10) (σ = 1.6)
APL-2	048572 3881376	2	Hematite (50%), pyrite (30%), chalcopyrite (15%), covellite (5%)	1223 (n=10) (σ =488)	14.4 (n=10) (σ = 12.6)	906 (n=6) (σ =922)	8.5 (n=6) (σ = 6.8)
APL-3	048574 3881377	2-3	Pyrite (48%), chalcopyrite (30%), hematite (20%), covellite (2%)	1098 (n=12) (σ =837)	11.7 (n=12) (σ = 10.0)	1991 (n=6) (σ = 1246)	5.6 (n=6) (σ =6.9)

APL-4	048574 3881384	4	Jasper (50%), pyrite (20%), hematite (15%), chalcopyrite (10%), covellite (5%)	579 (n=12) (σ = 641)	17.5 (n=12) (σ =15.0)	1012 (n=6) (σ =801)	9 (n=6) (σ = 9.8)
APL-5	048574 3881384	1	Pyrite (60%), Hematite (30%), chalcopyrite (10%)	204 (n=12) (σ = 443)	8.4 (n=12) (σ =10.9)	601 (n=6) (σ =233)	5.0 (n=6) (σ =4.2)
APL-6	048574 3881384	3	Chalcopyrite (40%), hematite (40%), pyrite (20%)	1649 (n=18) (σ = 627)	10.6 (n=18) (σ =7.6)	2014 (n=4) (σ = 1064)	9.0 (n=4) (σ = 11.9)
APL-7	048574 3881385	1	Hematite (55%), chalcopyrite (20%), pyrite (20%), jasper (5%)	177 (n=10) (σ = 123)	11.9 (n=10) (σ = 9.1)	1483 (n=6) (σ =879)	1.5 (n=6) (σ = 0.8)

Table 2:

Summary of average Se and Te concentration in chalcopyrite and pyrite by alteration stage. Detection limit: 9-15 ppm and 0.4-0.7 ppm for Se and Te respectively (histogram plots available in Appendix A6).

(ppm)	**Stage I**	**Stage II**	**Stage III**	**Stage IV**
Chalcopyrite				
Te	5	8	4	8
Se	601	1210	2215	1012
Pyrite				
Te	16	8	13	10
Se	182	1155	1862	532

Table 3:

Summary of average LA-ICP-MS spot data. Se is enriched in both chalcopyrite and pyrite at the South Apliki Breccia Zone compared to neighbouring Skouriotissa and 'All' VMS (*subset of 442 LA-ICP-MS spot analyses). Data shows that Se is preferentially incorporated into chalcopyrite whilst Te partitions strongly into pyrite.

Pyrite (ppm)	**Se**	**Te**	**Bi**	**Co**	**As**
Apliki	**922**	**11.2**	**2.5**	**268**	**152**
(n= 96)	σ 1004	σ 12.5	σ 5.6	σ 325	σ 165
Skouriotissa	**77**	**4.5**	**1.6**	**406**	**35**
(n= 54)	σ 129	σ 5.8	σ 2.7	σ 428	σ 93
All other VMS*	**55**	**6.7**	**7.1**	**245**	**469**
(n= 196)	σ 117	σ 15	σ 36	σ 640	σ 1585

Chalcopyrite (ppm)	Se	Te	Bi	Co	As
Apliki	**1576**	**4.5**	**0.6**	**4.9**	**5.1**
(n= 54)	σ 1069	σ 5.6	σ 2.1	σ 7.1	σ 13.7
Skouriotissa	**315**	**2.1**	**1.3**	**72**	**16**
(n= 27)	σ 361	σ 2.9	σ 1.8	σ 263	σ 60
All other VMS*	**77**	**1.9**	**0.8**	**1.3**	**8.6**
(n= 20)	σ 130	σ 2.6	σ 1.5	σ 8.1	σ 20